LBL-5214
c. 1

ATMOSPHERIC AEROSOL RESEARCH

ANNUAL REPORT 1975-76

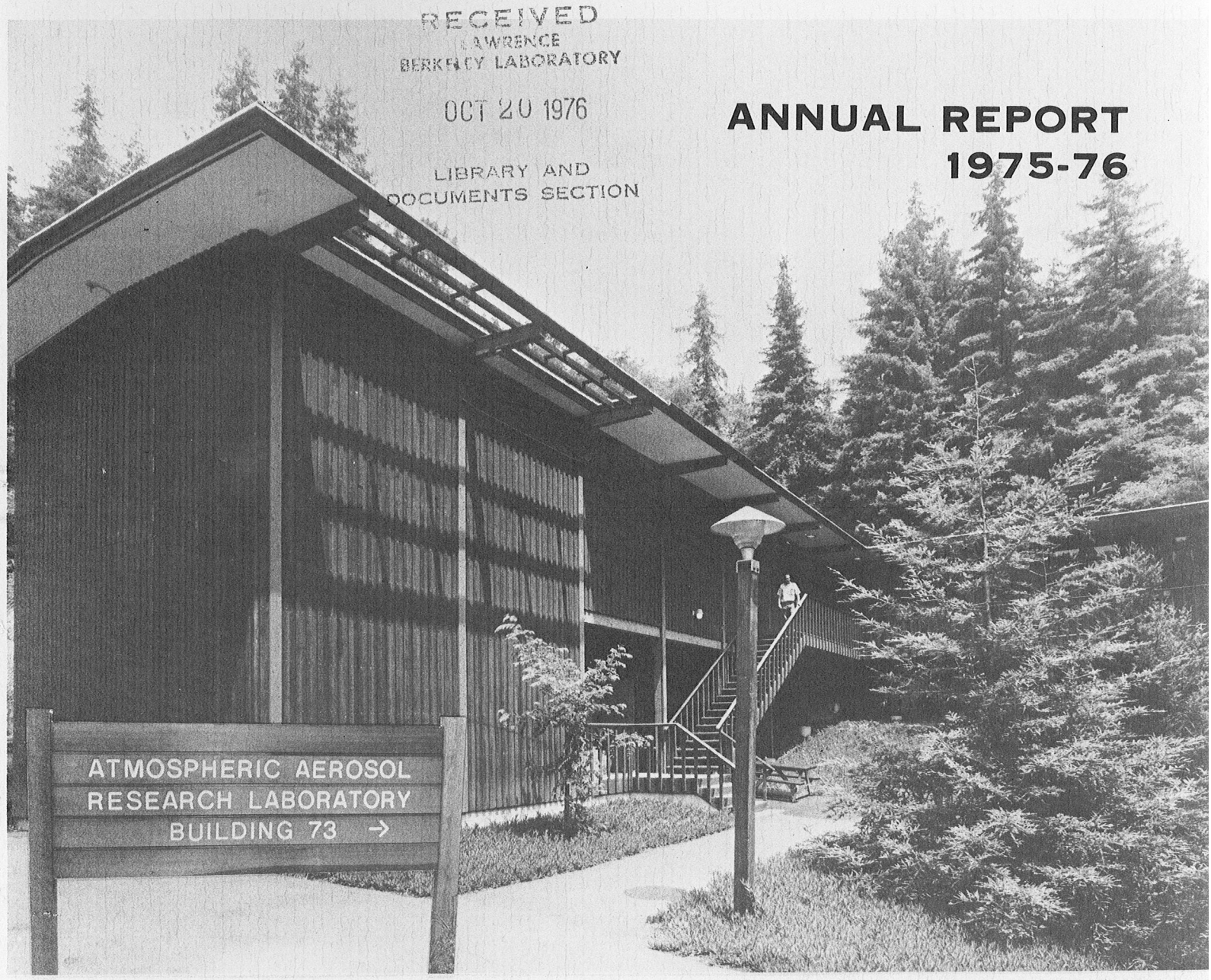

ENERGY AND ENVIRONMENT DIVISION
LAWRENCE BERKELEY LABORATORY UNIVERSITY OF CALIFORNIA, BERKELEY 94720

PREPARED FOR THE U.S. ENERGY RESEARCH AND DEVELOPMENT
ADMINISTRATION UNDER CONTRACT W-7405-ENG-48

LBL-5214
c. 1

LBL-5214

LAWRENCE BERKELEY LABORATORY
ENERGY AND ENVIRONMENT DIVISION
ATMOSPHERIC AEROSOL RESEARCH

ANNUAL REPORT
1975-76

PARTICIPANTS: T. Novakov, Principal Investigator
P. J. Bekowies*
S. G. Chang
M. Clemenson
R. L. Dod
R. D. Giauque
A. B. Harker†
C. D. Hollowell
L. Hughes#
S. S. Markowitz
P. J. Pagni**
H. Rosen
J. R. Wallace††

* Present address: 2135 Essex St., Berkeley, CA 94705.
† Present address: Science Center, Rockwell International, Thousand Oaks, CA 91360.
# NASA, Ames Research Center, Moffett Field, CA 94035.
** Department of Mechanical Engineering, University of California, Berkeley, CA 94720.
†† Present address: CDM/Limnetics, 11485 W. 48th Ave., Wheat Ridge, CO 80033.

TABLE OF CONTENTS

ACKNOWLEDGMENTS

The research described in this report is supported by the National Science Foundation--Research Applied to National Needs and the U.S. Energy Research and Development Administration. We would like to express our appreciation and thanks to Dr. Richard A. Carrigan and Dr. Robert P. Blaunstein, program managers of the respective agencies.

The Lawrence Berkeley Laboratory has provided funds for the construction of the Mobile Atmospheric Research Laboratory. For this we thank Dr. Andrew M. Sessler, Laboratory Director, Dr. Earl K. Hyde, Deputy Director, Dr. Jack M. Hollander, former Associate Director, Energy and Environment Division, and Dr. Robert J. Budnitz, Acting Head of the Energy and Environment Division.

We would also like to thank the following people:

Mr. E. R. Mayo, Highway Superintendent, California State Department of Transportation, Caldecott Tunnel, and his staff have helped us in every way possible to conduct the experiments in the Caldecott Tunnel.

Dr. Billy Loo of LBL has generously helped in the tunnel experiments by providing expert advice on aerosol sampling and by putting his dichotomous sampler at our disposal.

Messrs. Richard C. Schmidt, James H. Wise, Henry A. Brendel, and Gregory W. Traynor, and Ms. Jo Bea Way have provided superb technical help to the project.

Ms. Linda Wroth has done an excellent job in typing and editing this report.

INTRODUCTION

Aerosol particles (also referred to as particulate matter or particulates) play a major role in the air pollution problem. They are responsible for reduced visibility, acid rain, and in certain size ranges, are deposited in the lungs where they can cause a variety of adverse health effects. These particles can consist of solid and/or liquid substances. Some of these, such as windblown dust, soot, and flyash, originate in sources outside the atmosphere and are known as "primary" pollutants. Others are formed directly in the atmosphere by reactions among the primary particulate and gaseous species and are known as "secondary" pollutants. The nature of both these primary and secondary particulate species, as well as the extent to which atmospheric chemistry is governed by photochemical gas-phase mechanisms or catalytic gas-particle mechanisms, is presently a very active area of research.

In order to devise an effective control strategy, the particles responsible for the adverse environmental and health effects must be selectively identified and the process by which these species enter the atmosphere must be ascertained. In this regard one must distinguish two aspects of the analytical chemistry of atmospheric particulates. First we need to know the bulk chemical composition of any given sample of particulate matter. Some particles or some of their major bulk constituents may eventually be soluble in body fluids, so that practically their entire content can be toxicologically harmful. On the other hand, particle surfaces often are chemically dissimilar to the interiors of the particles. Particle surfaces carry microscopic layers of

contaminants that make contact with lung membranes, leading to exposures that have little to do with the bulk composition of the particles. A situation intermediate to the two extremes exists, when the harmful contaminants cover the surface of extremely small particles (of the order of 100 Å or less) which grow in the atmosphere as the result of coagulation. In this case the surface composition will be virtually undistinguishable from the bulk composition.

Most of the mass of atmospheric particulates consists of compounds of carbon, nitrogen, and sulfur. This illustrates the importance of pursuing earlier findings of the project that sulfur and nitrogen species, identical to those observed in the ambient air, can be synthesized in a few nonphotochemical reactions involving SO_2, NO, NH_3, and soot particles, which in many respects behave like activated carbon. The health effects of some of these species are unknown as of now. The carbon-bound sulfate is one such species. Others are the three or more reduced nitrogen forms such as amines, amides, and nitriles. The existence of these substances in the carbonaceous fraction of the atmospheric particulates requires that the composition and chemical fate of particulates be looked at in a new light. Namely, the results imply a strong suggestion that some of the sulfur and nitrogen forms are primary pollutants coming directly from sources, while others such as sulfate are essentially secondary pollutants but formed under catalytic action of chemically active primary particulates. This means that atmospheric sulfate pollution may be dominated, or significantly influenced, by processes of soot production, and that the chemical (and toxicological) properties of

atmospheric particulates may depend on the soot-bearing surface and/or bulk sulfur and nitrogen species.

The research on this project has continued along two parallel and interrelated approaches. The first approach is to prepare an inventory of chemical species found in various ambient and source-enriched particulates, and to study the relationship between the particulate species and the concentrations of concomitant gaseous pollutants and meteorological parameters. The second approach is to conduct laboratory experiments to elucidate various gas-particle reactions and to assess the role and significance of these processes in atmospheric pollution.

The main research tool for the characterization of particulate samples has been X-ray photoelectron spectroscopy (ESCA-Electron Spectroscopy for Chemical Analysis). The systematic chemical characterization of particulates by means of ESCA continued to be an ongoing activity during the last year's work on the project (Section I). Most of the samples used for this purpose were from St. Louis (obtained from Dr. T. Dzubay of EPA-Research Triangle Park, N.C.) and from the Caldecott Tunnel (collected by the project investigators). In addition to these, a number of California samples were also analyzed. Also, during the past year the infrared and Raman scattering techniques have been incorporated into the program and have yielded some rather interesting results (Sections I and II). The X-ray fluorescence technique has been used for elemental analysis, and preliminary measurements of the feasibility of using activation analysis for a determination of the light elements has been made (Section I). These instrumental techniques have

been complemented by wet chemical and microanalytical methods. A field program was also initiated last year with the construction of a Mobile Atmospheric Research Laboratory (MARL) which is now ready to make comprehensive measurements of gaseous and particulate concentrations in a field situation (Section III).

The present program can be divided into three main areas of research: chemical characterization of atmospheric aerosols, studies of reaction mechanisms, and field studies. The contributions made during the last year in each of these areas are described respectively in Sections I, II, and III of this report.

SECTION I

CHEMICAL CHARACTERIZATION OF ATMOSPHERIC AEROSOLS

Ammonium and Sulfate Species in Atmospheric Aerosols

R. L. Dod, S. G. Chang, and T. Novakov

The speciation of atmospheric aerosol particles is an important task because many of their environmental effects will depend on their specific chemical and physical state. Furthermore, it is important to determine the chemical compounds and species as they actually exist in the aerosol form and not as they may appear in aqueous solutions. Most analyses of pollution aerosol particles, however, have employed wet chemical methods which only reflect the chemical composition in solution. Primarily on the basis of these measurements, different workers have concluded that the principal sulfur and nitrogen species are sulfate (SO_4^{--}), nitrate (NO_3^-), and ammonium (NH_4^+) ions,[1] and have suggested that the most likely combinations of these ions are ammonium nitrate, NH_4NO_3, and ammonium sulfate, $(NH_4)_2SO_4$.[2] In addition to these, nitric acid[3] and sulfuric acid[4,5] are also suspected to exist under certain circumstances. Wet chemical methods, of course, are of no use for insoluble aerosol species. Nondestructive physical methods are therefore preferred as means for chemical characterization of collected particles. X-ray photoelectron spectroscopy (ESCA) is one such method. For example, the application of this method has helped to uncover the presence of significant concentrations of reduced nitrogen species of the amino type ($-NH_2$) in pollution aerosol particles.[6] These species are not soluble in water or solvents such as benzene, and therefore could not be detected by wet chemical methods.

ESCA analysis enables not only the possibility of detection of specific ions and functional groups, but also their mutual relationship. This is achieved by the measurements of the ESCA chemical shift augmented by the determination of relative concentrations and study of the volatility properties of particulate species.

The capability of ESCA for a straightforward differentiation of different forms of atmospheric sulfates is illustrated in Figure 1, where the nitrogen (1s) and sulfur (2p) spectral regions of two ambient samples are shown. (One was collected in West Covina, California, in the summer of 1973; the other, in St. Louis, Missouri, in the summer of 1975.) The peak positions corresponding to NH_4^+, $-NH_2$, and SO_4^{--} are indicated. The solid vertical bar indicates the ammonium peak intensity expected under the assumption that the entire sulfate is in the form of ammonium sulfate. Obviously, the observed ammonium content in the West Covina sample is insufficient to account for the sulfate by itself. This is in sharp contrast with the St. Louis sample where the observed ammonium intensity closely agrees with that expected for ammonium sulfate.

These results demonstrate that ammonium sulfate in the aerosols can easily be distinguished from other forms of sulfate such as the one found in the West Covina case. Wet chemical analyses,[7] however, performed on West Covina samples collected simultaneously with the ESCA samples resulted in ammonium concentrations substantially higher than those suggested by the ESCA measurements. This apparent discrepancy between the two methods was subsequently explained by the volatility of some ammonium species in the ESCA spectrometer vacuum.[8,9] That

these volatile losses are not caused by the volatilization of ammonium sulfate is evidenced by the St. Louis case, where no volatile losses were observed. Similarly, ammonium nitrate (negligible in these samples) and ammonium bisulfate were found to be stable in vacuum during the time periods usually required to complete the analysis. Therefore, species other than these have to be responsible for the apparent loss of ammonium in vacuum.

That the volatile ammonium is not necessarily associated with sulfate or nitrate ions is illustrated by means of results represented in Figure 2. Here the changes in the nitrogen (1s) spectrum of a sample collected in a highway tunnel[10] are shown as a function of the sample vacuum exposure time. Obviously, the ammonium peak intensity decreases with the vacuum exposure time of the sample. The amino-type nitrogen species intensity remains constant, however. The amount of nitrate in this sample was negligible compared to ammonium. The maximum ammonium peak expected under the assumption that the entire sulfate is ammonium sulfate is indicated by the solid vertical bar in Figure 2. It is obvious, therefore, that the counterions for this ammonium are neither nitrate nor sulfate.

Figure 3 summarizes the findings about ammonium volatility in the three samples discussed above. The shaded bars at the far left of the figure indicate the expected ammonium intensity based on the assumption that all of the sulfate in the sample is in the form of ammonium sulfate. It is evident from the figure that only the St. Louis sample contains ammonium sulfate, while the West Covina and the tunnel samples

contain a different kind of ammonium which volatilizes in the spectrometer vacuum.

We have applied this procedure routinely to analyze a number of ambient samples. Results of such measurements for six St. Louis samples are shown in Figure 4, where the ratio of the observed ammonium peak intensity to the peak intensity expected if the ammonium were in the form of ammonium sulfate is plotted as a function of the sample vacuum exposure time. From inspection of this figure, it is evident that in addition to the cases of practically stoichiometric ammonium sulfate (samples 913 and 914), there are those where the observed ammonium is found in excess of ammonium sulfate. The excess ammonium consists of volatile ammonium species which decay away until ammonium sulfate is the only ammonium species left (sample 917).

The anions corresponding to the volatile ammonium species cannot be identified with certainty at this time. One possibility is that these species are produced by the adsorption of ammonia on fine soot particles to form carboxyl- and hydroxyl-ammonium complexes which have been shown to have similar volatility properties to ambient particulates.[8] Another possibility is that these species could be due to ammonium halides which are also volatile in vacuum. More experimental work is necessary in order to evaluate these as well as other possibilities for explaining these volatile ammonium species.

References

1. C. E. Junge, Atmospheric Chemistry and Radioactivity, Academic Press, New York (1973).

2. G. M. Hidy and C. S. Burton, Int. J. of Chem. Kinetics, Symposium, 1, 509 (1975).

3. D. F. Miller and C. W. Spicer, J. Air Pollut. Contr. Assoc. 25, 940 (1975).

4. R. J. Charlson et al., Science 184, 156 (1974).

5. P. T. Cunningham et al., Chemical Engineering Division-Environmental Chemistry Annual Report, Argonne National Laboratory Report ANL-75-51 (1975).

6. T. Novakov et al., J. Colloid Interface Sci. 39, 225 (1972).

7. C. W. Spicer, private communication.

8. S. G. Chang and T. Novakov, Atmospheric Environment 9, 495 (1975).

9. B. R. Appel et al., Intern. J. Environ. Anal. Chem. 4, 169 (1976).

10. C. D. Hollowell et al., this report.

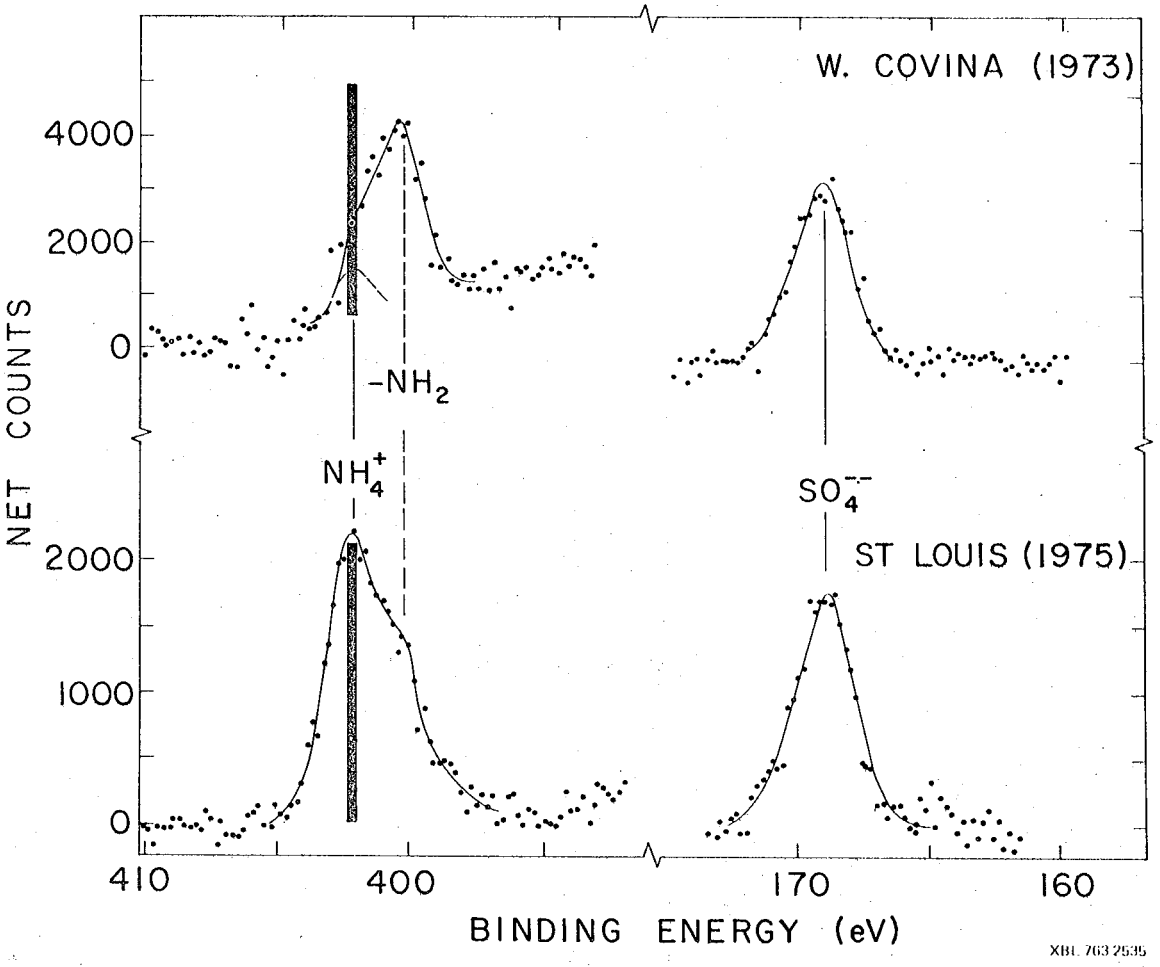

Figure 1. Nitrogen (1s) and sulfur (2p) regions in X-ray photoelectron spectra of two ambient samples. The peak positions corresponding to NH_4^+, $-NH_2$, and SO_4^{--} are indicated. The solid vertical bar represents the ammonium intensity expected under the assumption that the entire sulfate is in the form of ammonium sulfate. The difference in the relative ammonium content of the two samples is obvious. The sulfate and ammonium intensities in the St. Louis sample are compatible with ammonium sulfate. The ammonium content in the West Covina sample is insufficient to be compatible with ammonium sulfate. Both samples were exposed to the spectrometer vacuum for about one hour.

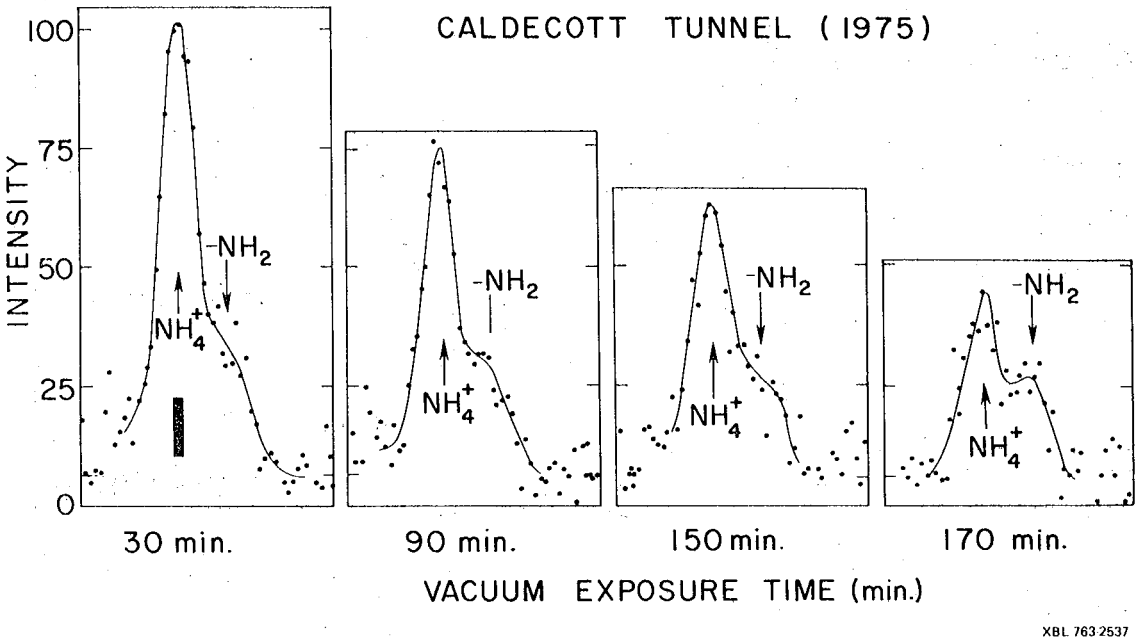

Figure 2. The variation in the observed ammonium peak intensity with vacuum exposure for a sample collected in a highway tunnel. The decrease in the peak intensity is caused by the volatilization of the ammonium species present in the sample. The solid vertical bar represents the ammonium intensity expected under the assumption that the sulfate in this sample is in the form of ammonium sulfate. The ammonium in this sample is considerably in excess of that expected for ammonium sulfate or ammonium nitrate.

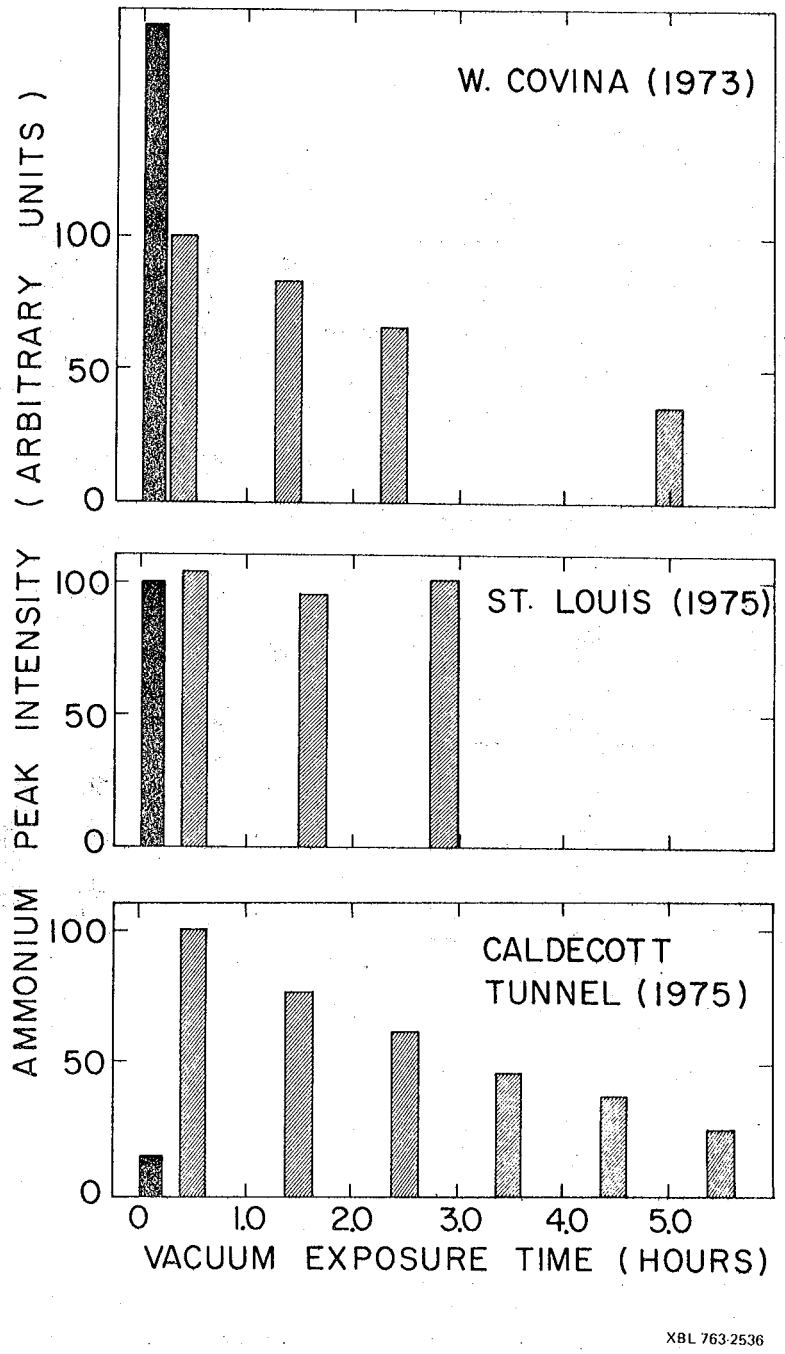

Figure 3. Volatility properties of West Covina, St. Louis, and automotive ammonium aerosol. The shaded bars on the far left of the figure indicate the expected ammonium intensity if the entire sulfate were ammonium sulfate.

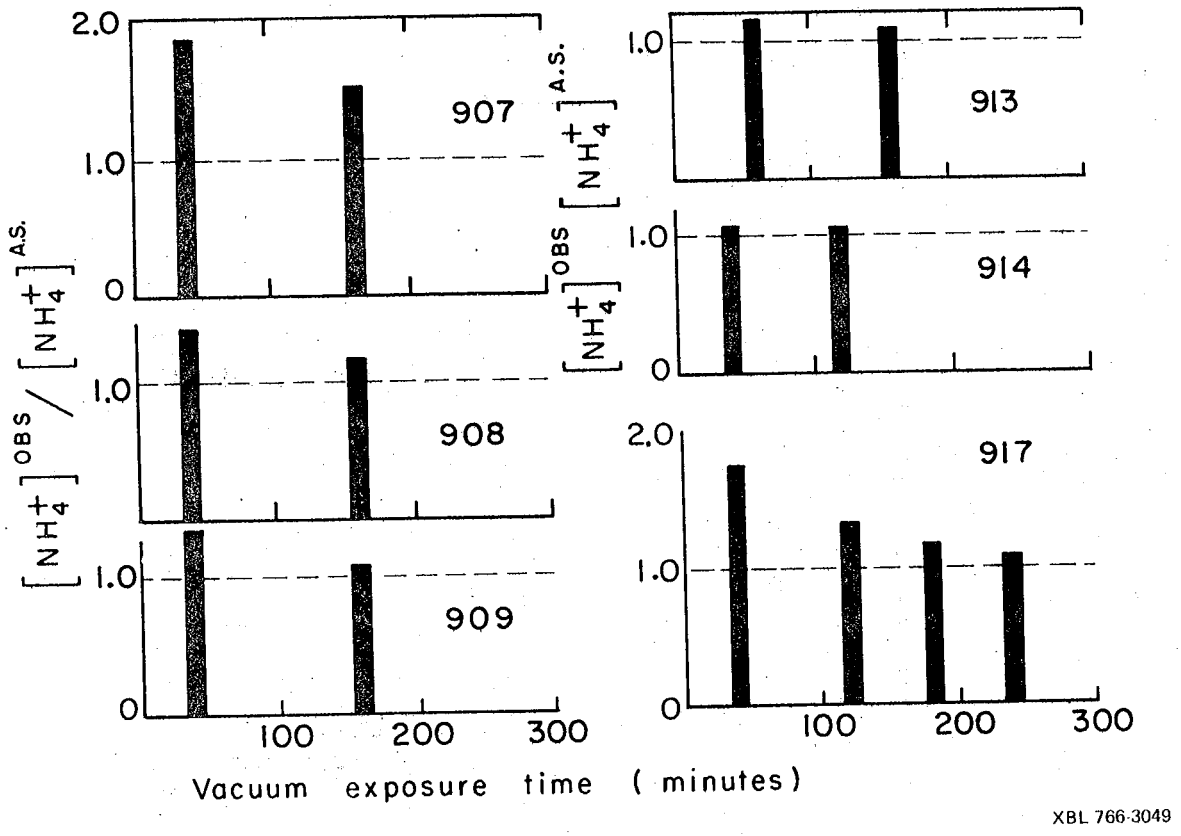

Figure 4. Volatility properties of ammonium in six ambient St. Louis samples. The ratio of the observed ammonium peak to the one expected under the assumption that the entire sulfate in these samples is ammonium sulfate vs. vacuum exposure time is shown. Note the cases of apparently stoichiometric ammonium sulfate (samples 913 and 914) and the cases where the volatile ammonium component is found in excess of that required for ammonium sulfate.

Application of Raman Scattering to the Characterization of Atmospheric Aerosol Particles

H. Rosen and T. Novakov

Considerable effort has been expended in the analysis of atmospheric particulates. Such techniques as wet chemistry, X-ray fluorescence, infrared spectroscopy, and ESCA have been used rather extensively. Yet there are still great uncertainties as to the chemical form and origin of many of the particulate species. During the last year we have performed preliminary studies to explore the feasibility of characterizing particulate pollutants by means of Raman spectroscopy. We believe that this is the first attempt to apply this spectroscopic technique in this area of research. The samples studied were, among others, polycrystalline graphite, activated carbon, diesel exhaust particles, automobile exhaust particles (unleaded fuel, no catalytic converter), and several ambient air samples.

In Figure 1 we show the Raman spectrum obtained from automobile exhaust. Similar spectra were observed for diesel exhaust, activated carbon, and polycrystalline graphite. The major features of the Raman spectrum are two intense lines at $\sim$ 1350 cm^{-1} and $\sim$ 1600 cm^{-1}. In the ambient samples, where the signal to noise is severely limited by the large fluorescence background, the only lines that were clearly seen above the noise level were also in this spectral region. In Figure 2 we show the Raman spectrum for the various samples in the region between 1200-1700 cm^{-1}.

In perfectly ordered single crystal graphite specimens only the Raman mode near 1600 cm^{-1} is observed and from a group theoretical analysis has been assigned to the k = 0,E_{2g} phonons of the graphite lattice.[1] The mode near 1350 cm^{-1} appears only in samples which are not perfectly ordered, and its intensity relative to that of the one near 1600 cm^{-1} varies inversely with the crystallite size, L_a, as obtained from X-ray data.[1]

It is evident from Figure 2 that the spectra of activated carbon, diesel exhaust, automobile exhaust, and ambient samples are very similar. The positions of the two Raman modes in these spectra are coincident to within ± 10 cm^{-1}, which is the estimated error. Since the phonon frequencies are a sensitive probe of the lattice, we suggest that these spectra give strong evidence for the existence of physical structures similar to activated carbon in the samples studied.

Using the available results from the literature,[1] we can estimate the crystallite sizes in the various samples from the intensity ratios of the two observed Raman modes. The ambient, diesel exhaust, and automobile exhaust particles appear to have roughly the same peak intensity ratio, yielding crystallite sizes between 50 and 100 Å.

Our results indicate that physical structures similar to activated carbon are present in exhaust and ambient samples. The fact that the two observed modes are the dominant features of the Raman spectrum may indicate that "graphitic" soot is the major component in these samples. However, the large intensity of these modes may be due just to their large Raman cross section. Quantitative interpretation of these results

will have to await a more detailed analysis. Such analysis will have to include measurements of the Raman cross section, the optical absorption cross section, and also take into account the little-understood particle size effects.

References

1. F. Tuinstra and J. L. Koenig, J. Chem. Phys. 53, 1126 (1970).

2. F. S. Goulding, J. M. Jaklevic, and B. M. Loo, Report UCID-3767, Lawrence Berkeley Laboratory, University of California, Berkeley, CA 94720; Report EPA-650/2-75-048, U.S. Environmental Protection Agency, Washington, DC 20460 (April 1975).

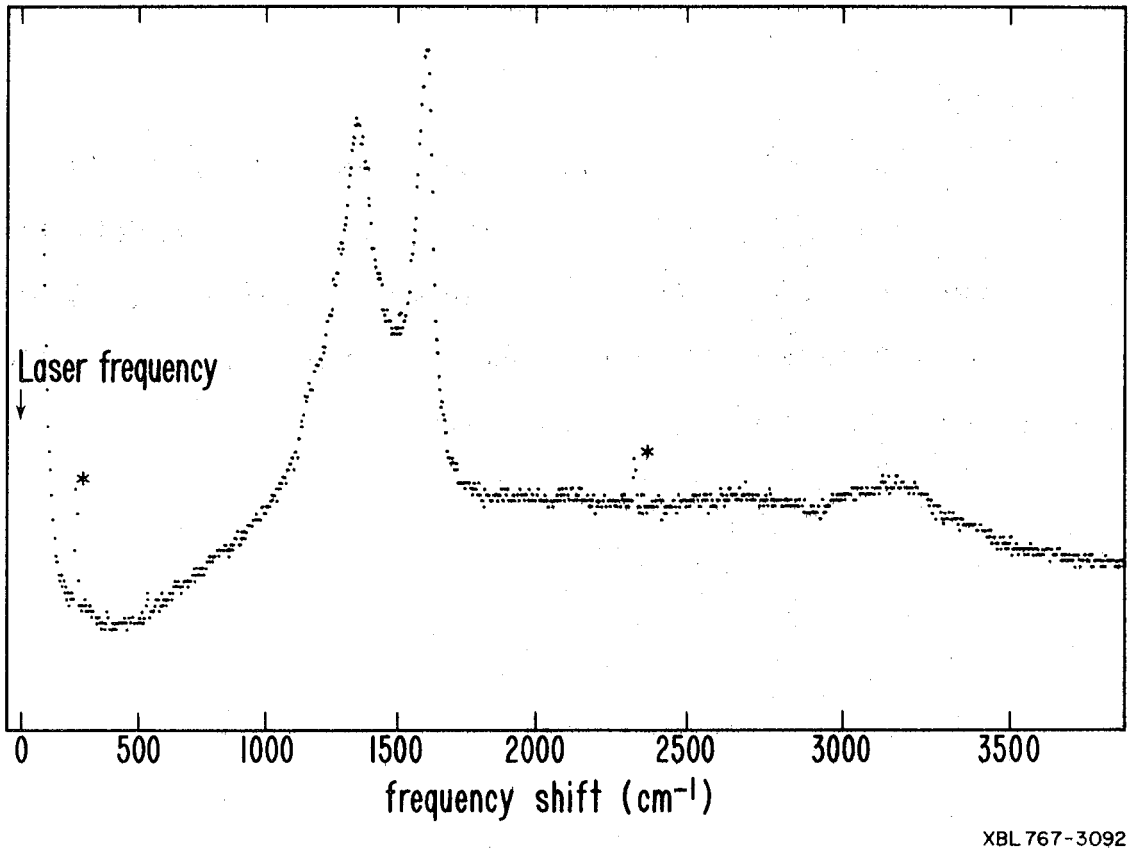

Figure 1. Raman spectrum of automobile exhaust in the spectral region between 90 and 3830 cm^{-1}. The sample was collected from 100 cold starts of a 1974 Pinto using lead-free gas and having no catalytic converter. The slit width for this scan was 3 Å. The lines identified with an asterisk are due to grating ghosts.

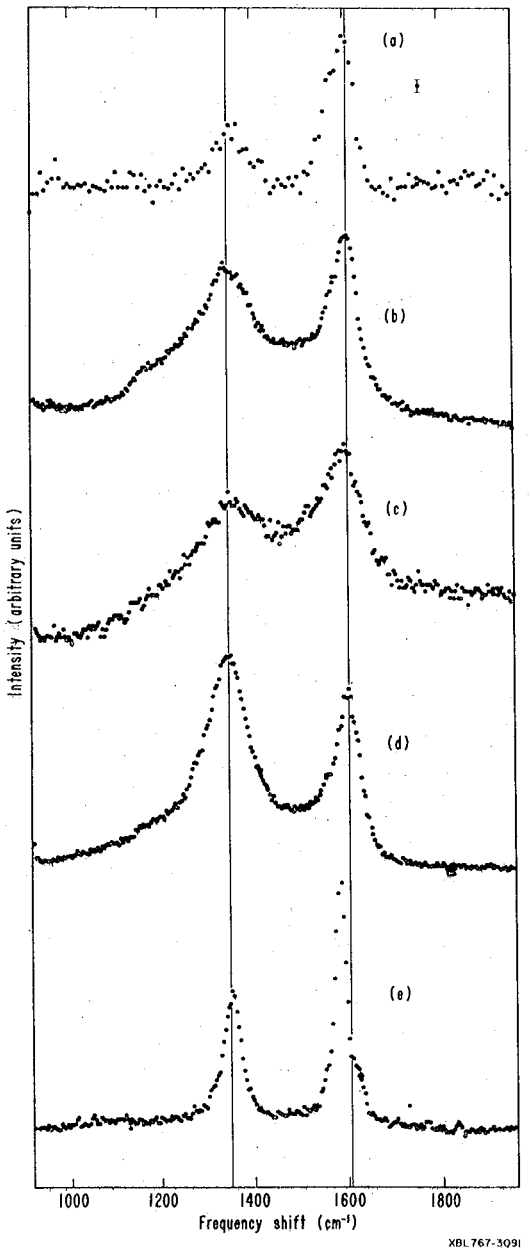

Figure 2. Raman spectra between 1200 and 1700 cm^{-1} of a) ambient sample collected in 1975 as part of the RAPS program (The sample was collected on a dichotomous sampler[2] and was in the small size range fraction.); b) automobile exhaust collected from 100 cold starts of a 1974 Pinto using lead-free gas and having no catalytic converter; c) diesel exhaust; d) activated carbon; and e) polycrystalline graphite. The slit width for samples b-e was 3 Å; while for sample a, 7-Å slits were used to improve signal to noise.

Nuclear Activation Analysis for Low-Z Elements in Atmospheric Aerosol Particles

M. Clemenson, S. S. Markowitz, and T. Novakov

The X-ray fluorescence technique has proved to be a powerful tool for a determination of heavy elements in ambient aerosol particles. However, its sensitivity is severely limited for light elements ($Z < 11$) by X-ray absorptive effects and low fluorescent yields. We have been investigating the feasibility of using activation analysis for a determination of the concentration of these light elements which comprise a major fraction of airborne particulates. Our initial experiments involve the detection of elemental nitrogen using protons to induce the reaction $^{14}N(p,\alpha)C^{11}$ and then monitoring the positron annihilation from C^{11}. In these experiments there is no interference from carbon because of the high threshold (20.3 MeV) for production of ^{11}C from ^{12}C.

A compound with a known amount of nitrogen, Melamine ($C_3N_6H_6$) was prepared by vacuum sublimation onto 0.001-in. Al foils. The Melamine thicknesses for the various samples were either 1.5 mg/cm^2 or 3.2 mg/cm^2. Of this, 66.7% by weight is N. A stack of these foils was irradiated for 3.8 min in the LBL 88-in. cyclotron at a beam intensity of $\sim$ 1.4 μA of protons. The maximum beam energy was 21.0 MeV, and known range-energy relationships were used to calculate the proton energy incident upon each target. Aluminum foils were used to degrade the beam energy. The target stack was water-cooled. The beam was collimated to a diameter of 3/8 in.

Radioactive ^{11}C, a positron emitter with a half-life of 20.4 min, was conveniently counted for its 511-keV annihilation radiation by means of a Ge(Li) multichannel spectrometer. A spectrum in the region near 511 keV is shown in Figure 1. The decay of the integrated intensity in this peak for one of the target foils is shown in Figure 2. The 20-min half-life of ^{11}C is clearly observed for several decades. After the ^{11}C has decayed away, the decay curve indicates 511-keV radiation from longer-lived species, probably 15-hr ^{24}Na and 18-hr ^{55}Co. [Other γ-rays have been identified from these nuclides; they arise from the (n,α) reaction on trace impurities of Fe in the Al backing foil.] Counts were also taken with a 511-511 coincidence unit and with beta proportional counters. The count rates with the Ge(Li) system were quite high even at shelf 14 ($\sim$ 5 in. from the detector). The overall detection coefficient (peak count rate/disintegration rate) was measured with a standard source of ^{22}Na. It was 9.5×10^{-4}.

Measured count rates were corrected back to end-of-bombardment, A_0, converted to disintegration rates, D_0, and the cross sections were calculated for each foil. The results are shown in Table I and Figure 3.

The measured count rates at a proton energy of 12.3 MeV and a bombardment time of 3.8 min at 1.4 μA yield a sensitivity of $\sim$ 0.1 $\mu g/cm^2$ for the detection of nitrogen, provided that other impurities do not give both a similar γ energy and half-life to that of ^{11}C. Therefore, the (p,α) activation for N seems promising. Irradiations of synthetic and actual aerosol filter samples will be carried out to examine the proton activation procedure.

Table I

Foil no.	E_p(MeV)	Cross sec. (mb)
1	20.1	71
2	15.1	89
3	12.3	76
4	9.2	60
5	6.0	66
6	3.9	1.9

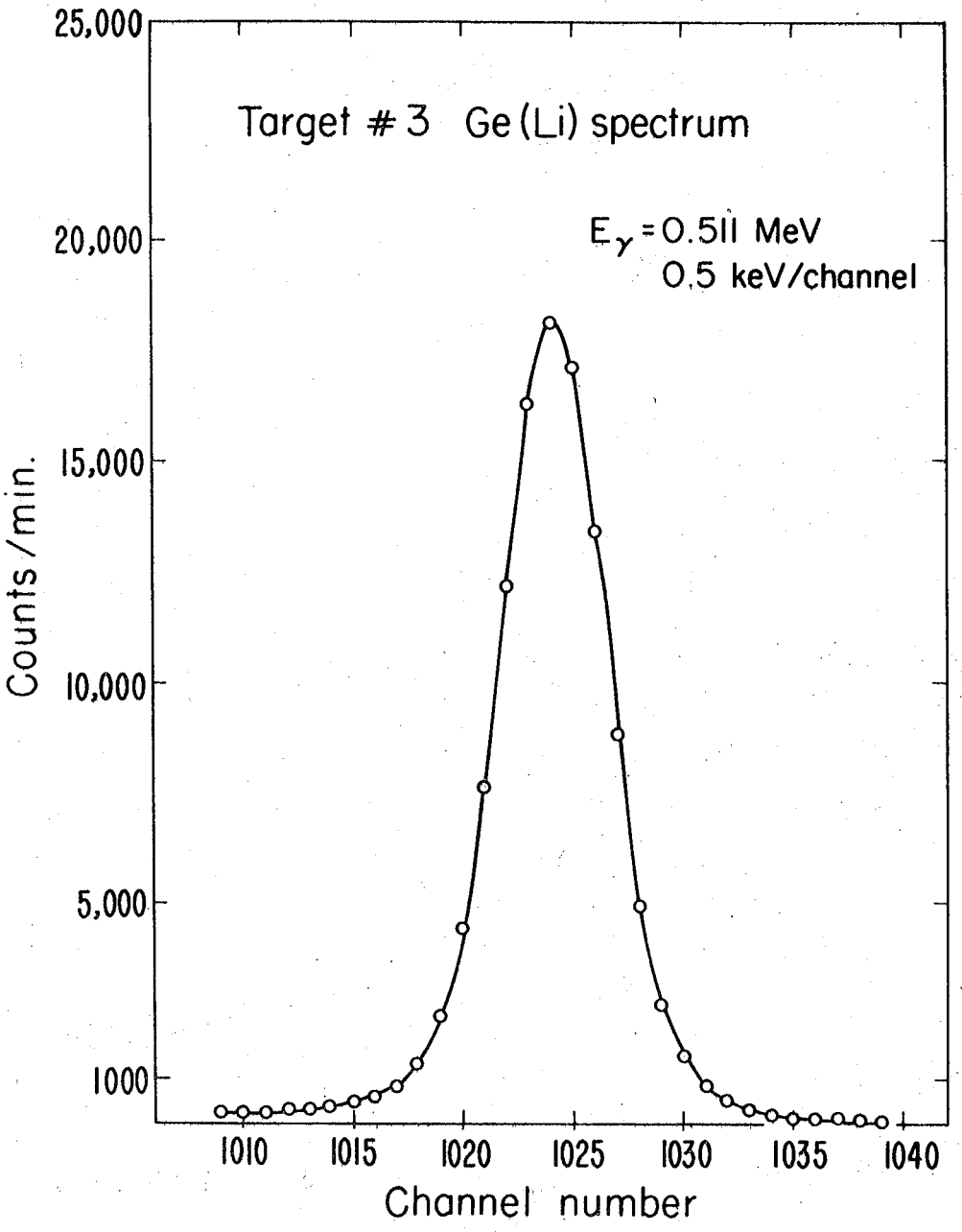

Figure 1. Ge(Li) spectrum near 511 keV.

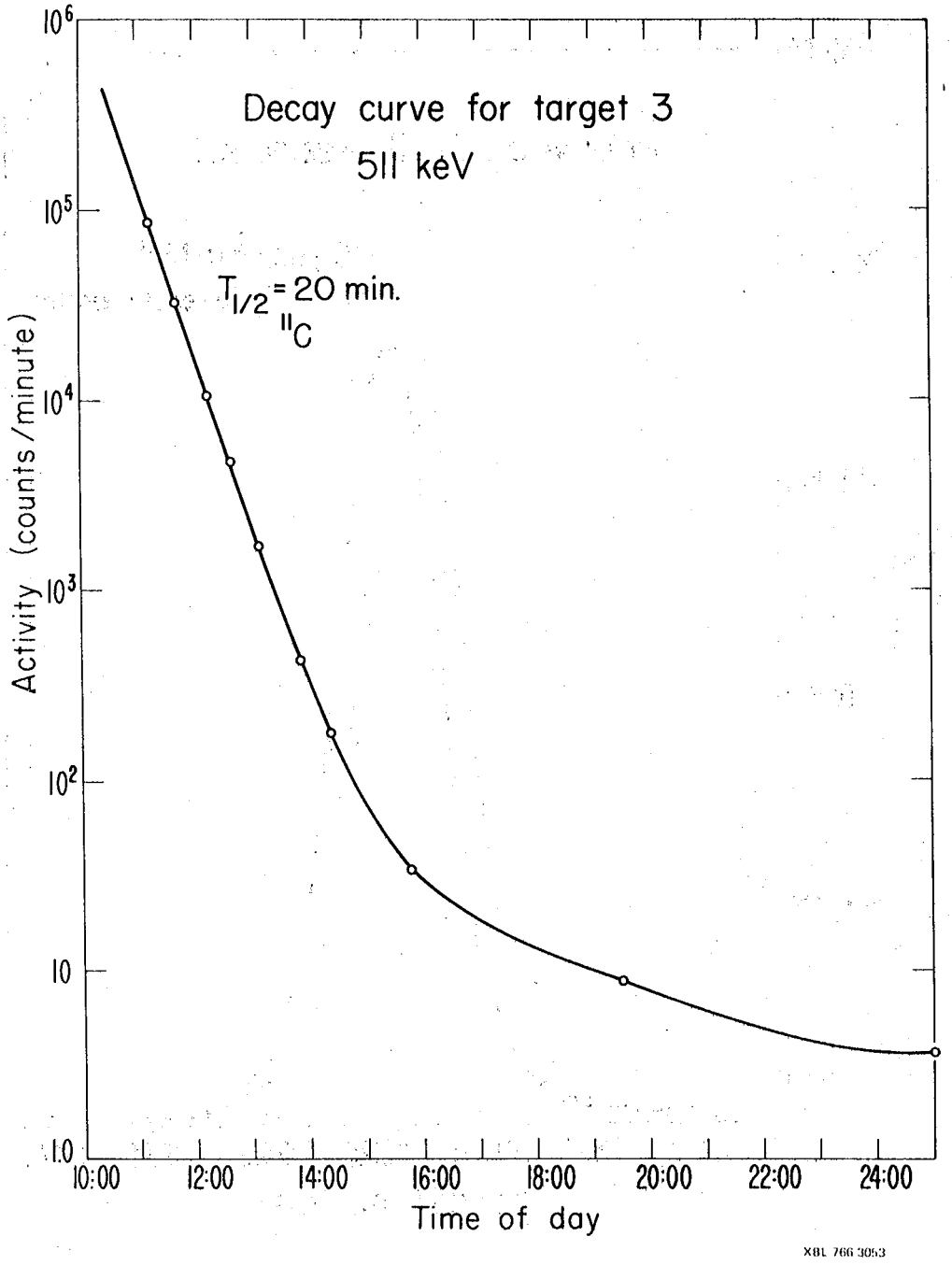

Figure 2. Decay of the 511-keV peak from ^{11}C produced by 12.3-MeV protons.

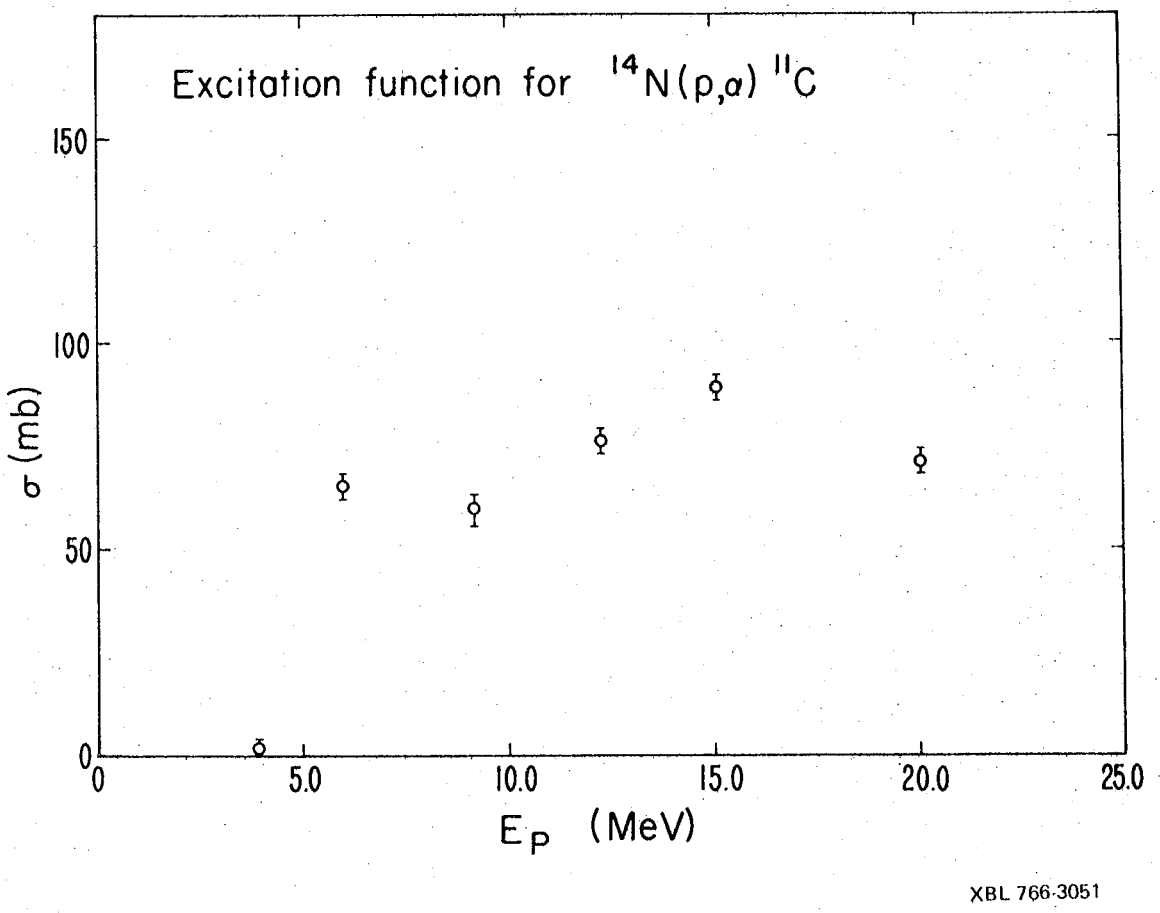

Figure 3. Excitation function for the $^{14}N(p,\alpha)^{11}C$ reaction.

Manganese Emissions from Combustors*

A. B. Harker, P. J. Pagni, T. Novakov, and L. Hughes

Undesirable emissions from aircraft, automotive, and stationary gas turbine engines are produced in the combustion chamber with no significant change during subsequent flow through the turbine. These emissions can therefore be characterized by studying model combustion chamber[1] exhaust. The apparatus used has previously been described in detail.[2,3] Emphasis is therefore placed on results obtained using X-ray photoelectron spectroscopy to analyze particulate exhaust collected from a model combustor burning JP-4 with 2-methyl cyclopentadienyl manganese tricarbonyl (MMT) added in concentrations ranging from 0 to 0.25% by volume. It is desired to determine the oxidation state and physical form of the manganese after combustion as well as its effect on other particulate emissions.

X-ray photoelectron spectroscopy (XPS) consists of determining the binding energy of photoelectrons expelled from a sample irradiated with monoenergetic X-rays.[4] Applications of the technique to particulate analysis have been reported.[5] The electron binding energies obtained are characteristic of the element observed, with the precise value of these energies being modified by the valence electron distribution of the molecule in which the observed atom exists. The difference in electron binding energy between the elemental and molecular forms of

*Published in Chemosphere 6, 339 (1975) and as LBL-4403.

an atom is known as the chemical shift. These shifts are correlated to the effective charge an atom possesses in a molecule and are used to establish oxidation states. The oxidation states of manganese, however, have such small chemical shifts that it is difficult to unambiguously assign an effective charge from a measurement of the chemical shift alone.

Because of this difficulty, the multiplet splitting effect was employed here to determine the oxidation state. Multiplet splitting of core electron binding energies has been observed in the photoelectron spectra of transition metal compounds and other paramagnetic species.[6] In any atomic or molecular system with unpaired valence electrons the 3s-3d exchange interaction effects the core electrons differently, according to the orientation of their spin. This causes the 3s core level to be split into two components. For an Mn^{2+} ion whose ground state configuration is $3d^5$ ^6S the two multiplet states will be ^7S and ^5S. In an Mn^{4+} ion having the ground state configuration $3d^3$ ^4F the two spectroscopic states will be ^5F and ^3F. The magnitude of the multiplet splittings should in first approximation be proportional to the number of unpaired 3d electrons. Hence the Mn(3s) splitting will be greatest for Mn^{2+} ions, and least for Mn^{4+}.

A photoelectron spectrum of the exhaust particles in the binding energy range 0 to 670 eV is shown in Figure 1. The major constituents are manganese, carbon, and oxygen, with trace amounts of nitrogen and sulfur. The Mn(3p) level was used for the chemical shift measurements while the Mn(3s) level provided the multiplet splitting data. Mn(3p) binding energies have been determined for the exhaust particle samples

and for the compounds MnO, Mn_2O_3, Mn_3O_4, and MnO_2. These values, corrected for sample charging using the hydrocarbon contaminant with a C(1s) binding energy of 285.0 eV, are listed in Table I. Clearly it cannot be determined on the basis of chemical shift alone whether the oxidation state is MnO, Mn_3O_4, or Mn_2O_3.

The oxidation state assignment is made by examining the multiplet splittings of the 3s electron level in spectra such as those shown in Figure 2. MnF_2 is included since it is the most ionic compound of divalent manganese and therefore its Mn^{2+} ion must exhibit the largest possible 3s multiplet splitting. Mn(3s) spectra were also obtained for Mn_3O_4 and Mn_2O_3. A summary of the measured multiplet splittings along with values from the literature is given in Table II. Based on the excellent agreement between the exhaust particulate and MnO multiplet splitting magnitudes, it is concluded that the oxidation state of the manganese in the combustor exhaust is +2 as MnO. Other Mn^{2+} compounds are eliminated by the fact that oxygen is the only negatively charged species present in sufficient concentration to stoichiometrically balance the manganese. XPS measurements of atomic ratios in the exhaust sample showed that the ratio of sulfur to carbon atoms increased from 0.047 for pure JP-4 fuel to 0.145 when the additive was used. It has been demonstrated[10] that MMT strongly influences the size distribution in the exhaust, producing many more small particles. The resulting increase in the surface area available for heterogeneous reactions could explain the increase in the sulfur-to-carbon ratio.[11]

It is interesting to note that the manganese oxide in the exhaust

particles was stable over long periods of time in the ambient atmosphere, whereas the reagent grade powdered MnO is readily oxidized. Only when heated to 500°C for 10 min in O_2 at 100 μ Hg total pressure was the monoxide in the exhaust sample observed to form higher oxides. The stability of the particulate manganese suggests that the MnO is intimately associated with other components of the exhaust particles. Since carbon is by far the most abundant constituent of the particles, it is likely that the manganese monoxide is trapped in carbonaceous material which may form a barrier against further oxidation.

A neutron activation analysis of the exhaust samples was also obtained[12] which indicated that all the manganese added to the fuel was emitted. Knowing the amount of manganese emitted and the oxidation state as MnO, the mass of manganese monoxide emitted can be calculated. Since the total mass of particulate emissions is also measured, the mass of carbon emitted is immediately obtained. The resulting emission indices are shown in Figure 3 as a function of additive concentration. Small amounts of the additive, less than 0.01% (vol), decrease the emitted mass. However, at additive concentrations greater than 0.01% (vol) both the total mass and the mass of carbon emitted increase. The carbon emission index reaches a plateau as additive concentration increases at $\sim$ 1.7 gm/kgm fuel above the no-additive level. A carbon deposition rate of $\sim$ 1.6 gm/kgm of fuel has been reported for a similar combustor.[13] This leads to the conclusion that prohibition of carbon deposition within the combustion is the cause of the increased mass emission. Similar minimums in mass emissions at low additive concentrations have been observed for oil-burning furnaces[14] and power-generating turbines.[15]

References

1. R. F. Sawyer, in Emissions from Continuous Combustion Systems, E. S. Starkman, ed., Plenum, New York (1972), p. 243.

2. D. V. Giovanni, P. J. Pagni, R. F. Sawyer, and L. Hughes, Comb. Sci. Tech. 6, 107 (1972).

3. P. J. Pagni, L. Hughes, and T. Novakov, in Atmospheric Pollution by Aircraft Engines, AGARD Conf. Proc. No. 125, NATO, London, England (1973), p. 28-1.

4. J. M. Hollander and D. A. Shirley, Annual Review of Nuclear Science 20, 435 (1970).

5. T. Novakov, in Proc. Second Joint Conf. on Sensing Envir. Pollutants, Instr. Soc. of America (1974), p. 197.

6. C. S. Fadley, in Electron Spectroscopy, D. A. Shirley, ed., North Holland, Amsterdam (1972), p. 781.

7. G. K. Wertheim, S. Hutner, and H. J. Guggenheim, Phys. Rev. B7:1, 556 (1973).

8. C. S. Fadley, D. A. Shirley, A. J. Freeman, P. S. Bagus, and J. V. Mallow, Phys. Rev. Letters 23, 1397 (1969).

9. J. C. Carver, T. A. Carlson, L. C. Cain, and G. K. Schweitzer, in Electron Spectroscopy, D. A. Shirley, ed., North Holland, Amsterdam (1972), p. 803.

10. P. J. Pagni and L. Hughes, Chemosphere 1:5, 209 (1972).

11. T. Novakov, S. G. Chang, and A. B. Harker, Science 186, 259 (1974).

12. L. Hughes, "The Effect of a Manganese Fuel Additive on Air Quality," dissertation, Environ. Health Sci., School of Public Health, University

of California, Berkeley, 1973.

13. E. S. Starkman, A. G. Cattaneo, and S. H. McAllister, Indust. Engr. Chem. 43, 2822 (1951).

14. G. B. Martin, D. W. Pershing, and E. E. Berkau, Office of Air Programs Publication No. AP-87, U.S. Environ. Protection Agency, Research Triangle Park, N.C. (1971).

15. L. Plonsker, E. B. Rifkin, M. E. Gluckstein, and J. D. Bailie, "Reduction of Gas Turbine Smoke and Particulate Emissions by a Manganese Fuel Additive", Ethyl Corp., Ferndale, Michigan (1974).

Table I. Measured Mn(3p) electron binding energies.

Sample	Exhaust	MnO*	Mn_3O_4	Mn_2O_3	MnO_2
Binding energy (eV)	48.9 ±0.2	48.8 ±0.2	48.9 ±0.2	49.0 ±0.2	49.9 ±0.2

*Powdered reagent grade MnO which undergoes rapid surface oxidation at ambient conditions was used.[7]

Table II. Multiplet splitting of Mn(3s).

Compound	Splitting (eV)			
	This work	Wertheim et al.[7]	Fadley et al.[8]	Carver et al.[9]
MnF_2 (2+)	6.4 ±0.2	6.50 ±0.02	6.5	6.3
Exhaust particulate	6.1 ±0.2	—	—	—
MnO (2+)	—	6.05 ±0.04	5.7*	5.5*
Mn_3O_4 (2+ and 3+)	5.5 ±0.2	—	—	—
Mn_2O_3 (3+)	5.5 ±0.2	5.50 ±0.10	—	5.4
MnO_2 (4+)	4.6 ±0.2	4.58 ±0.06	4.6	—

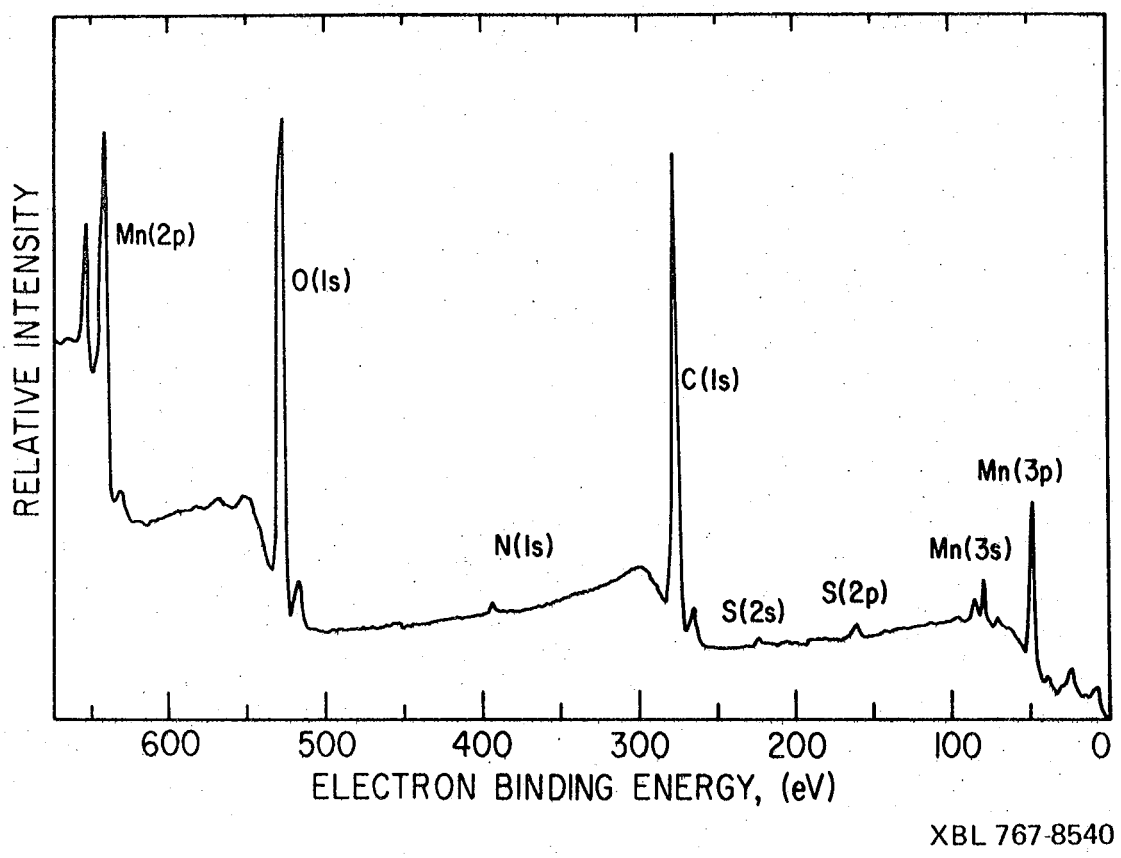

Figure 1. X-ray photoelectron spectrum of particles emitted by a model combustor burning JP-4 with 0.25% (vol) MMT and collected on a Nucleopore filter.

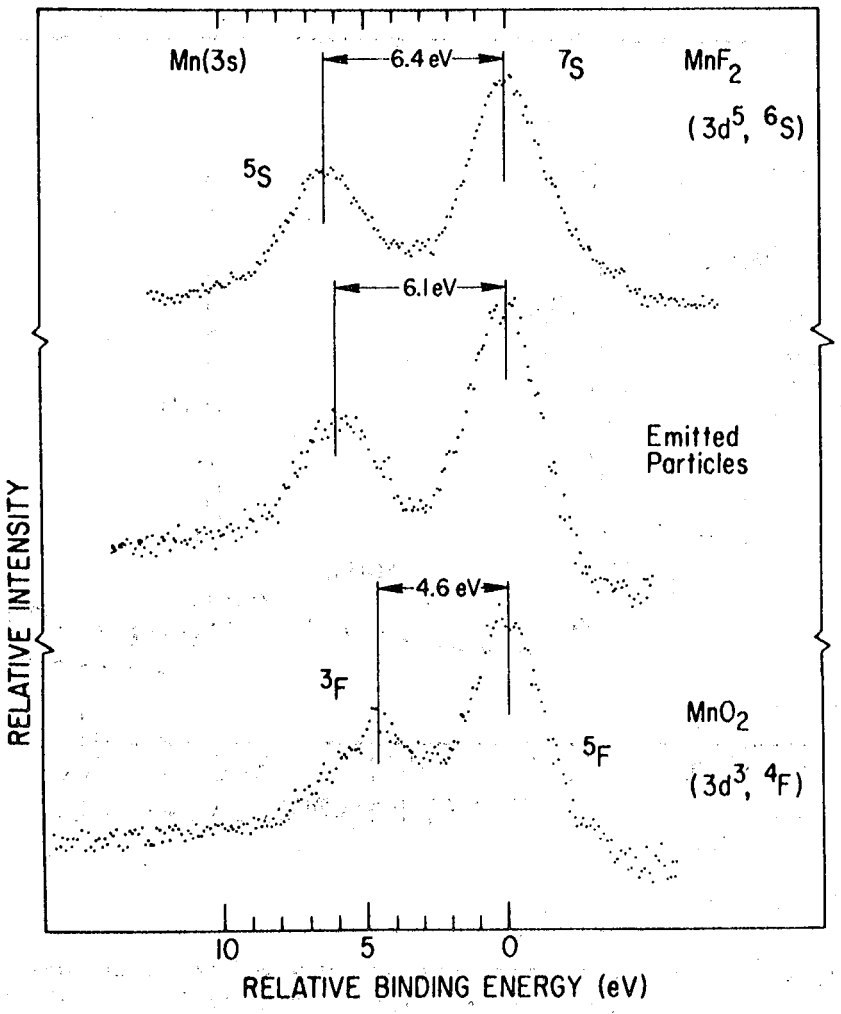

Figure 2. Comparative X-ray photoelectron spectra of 3s core levels for MnF_2, exhaust particles, and MnO_2 showing the multiplet splitting of the 3s level. It is concluded that MnO is the principal manganese oxide in the emitted particles.

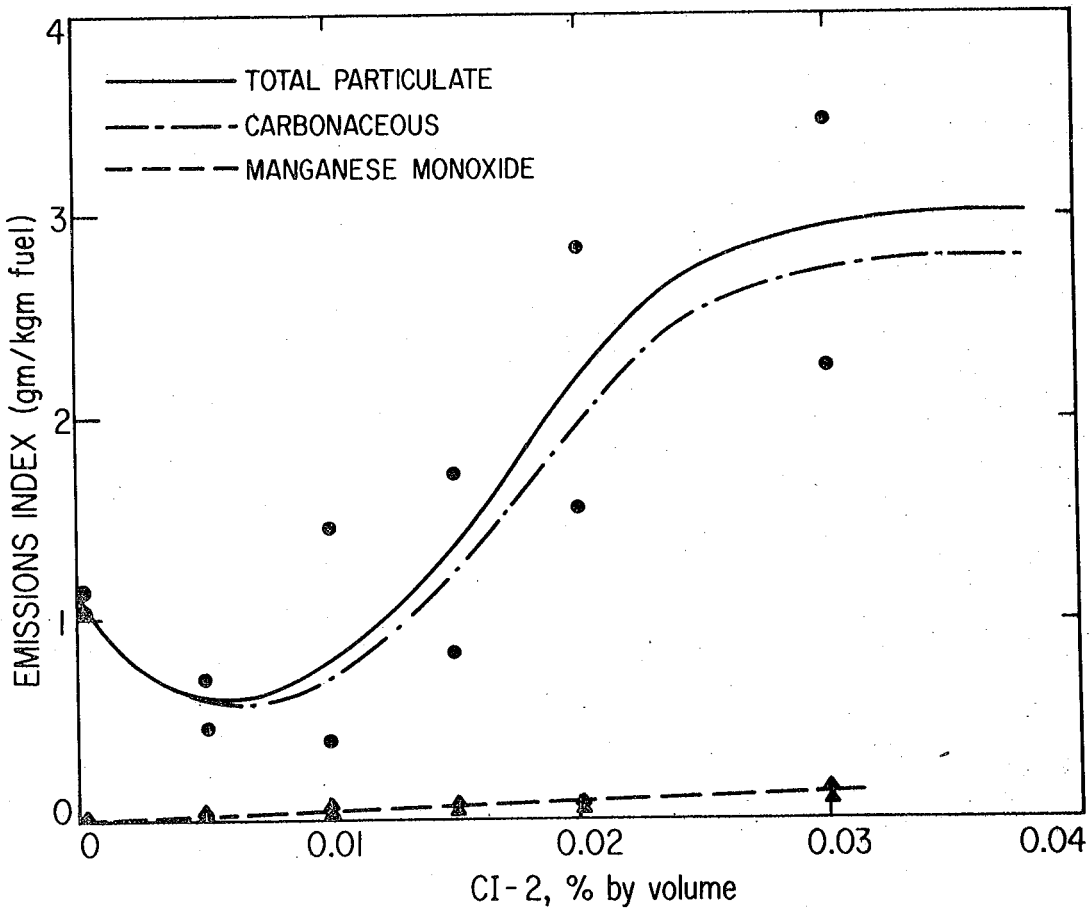

XBL 767-8539

Figure 3. Typical experimental results for the total particulate emission index. The solid line is an averaged total particulate EI. The carbonaceous EI is the difference between the total EI and the MnO EI.

SECTION II

STUDIES OF REACTION MECHANISMS

Infrared and Photoelectron Spectroscopic Study of SO_2 Oxidation on Soot Particles*

S. G. Chang and T. Novakov

Novakov et al.[1] have recently demonstrated that combustion-generated air-suspendable carbonaceous (soot) particles are an efficient catalyst for the oxidation of SO_2 to sulfate, and suggested that this heterogeneous oxidation is important from the air pollution standpoint. X-ray photoelectron spectroscopy (ESCA) and wet chemical methods were used to characterize the product of SO_2 oxidation. The results of ESCA analysis demonstrate that the oxidation state of this produce is 6+, i.e., sulfate, while wet chemical analyses show that the sulfate associated with soot particles is water soluble, yielding an acidic solution. The question about the actual state of chemical bonding of the sulfate associated with soot particles remained open, however. In order to gain a more complete understanding of the state of chemical bonding, we have applied both photoelectron and internal reflection infrared (IRS) spectroscopy to the analysis of the sulfate species produced catalytically on soot particles.

Photoelectron spectra were obtained with an AEI-200 photoelectron spectrometer utilizing Al K_α (1486.6 eV) radiation. IRS measurements were obtained by means of a Perkin-Elmer 621 infrared spectrophotometer equipped with a Wilks IRS attachment. Interaction of SO_2 with soot

---

*Accepted for publication in J. Colloid Interface Sci.; condensed version of Lawrence Berkeley Laboratory Report LBL-4446 (1975).

particles was studied either in a static regime, i.e., with soot particles precollected on a filter with subsequent exposure to SO_2 at room temperature, or in a flow system by introducing SO_2 downstream from a propane flame.

Photoelectron spectra representing the sulfur (2p) and carbon (1s) regions of propane soot particles produced by a Bunsen burner are shown in Figure 1a. The S (2p) photoelectron peak at a binding energy of 169 eV corresponds to sulfate. The C (1s) peak appears essentially as a single component line and corresponds to a mostly neutral charge state consistent with the soot structure. It is of interest to note that even the combustion of very low sulfur content fuels (0.005% by weight) results in the formation of easily detectable sulfate emission.

The specific role of soot particles as a catalyst for the oxidation of SO_2 is demonstrated with the aid of Figure 1b. Here we show the S (2p) and C (1s) photoelectron peaks of soot particles, generated in analogous manner as before, but exposed to additional SO_2 in a flow system. A marked increase in the sulfate peak intensity, relative to carbon, is evident. The atomic ratio of sulfur to carbon in Figures 1a and 1b are about 0.15 and 0.50 respectively.

In order to understand the nature of the sulfate species formed on soot, infrared (IRS) spectra of the samples used for ESCA analyses (Figures 1a and 1b) were studied. The IRS spectra of these samples, in the spectral region between 1500 and 500 cm^{-1}, are shown in Figures 2a and 2b respectively. In Figure 2c the spectra in Figure 2b are expanded by a factor of 5 so that a better comparison can be made to the

spectrum of an aqueous solution of ammonium sulfate shown in Figure 2d. The absorption band near 1400 cm^{-1} is due to an ammonium vibration while the bands near 1080 cm^{-1} and 615 cm^{-1} are due to the ν_3 and ν_4 vibrations of the sulfate ion. It is clear from the figure that the spectra of ammonium sulfate and sulfate associated with soot are very similar. In contrast, these spectra are dissimilar to those of a 1N solution of H_2SO_4 and an aqueous solution of ammonium bisulfate shown in Figures 3a and 3b respectively.

It is possible to explain the observed differences in the IR absorption spectra of the various sulfate species by considering the major dissociation products of these compounds and their symmetry properties. Sulfuric acid is a strong acid. Its first ionization in water is virtually complete: $H_2SO_4 + H_2O \rightarrow HSO_4^- + H_3O^+$. Its secondary ionization constant in water is 1.2×10^{-2} (at 25°C). The dominant species in 1N sulfuric acid are therefore hydrogen sulfate anions (HSO_4^-) and hydronium ions (H_3O^+). Ammonium bisulfate will completely dissociate in water to form an ammonium cation and again a hydrogen sulfate anion: $NH_4HSO_4 \rightarrow NH_4^+ + HSO_4^-$. The principal species in an aqueous solution of ammonium bisulfate are, therefore, ammonium cations and hydrogen sulfate anions. In contrast, ammonium sulfate will completely dissociate in aqueous solution into ammonium cations and sulfate anions.

The observed frequencies of different sulfate anions and their assignment on the basis of a group theoretical analysis[2] are listed in Table I. An inspection of these data shows that the spectra of sulfate species produced by catalytic oxidation of SO_2 closely match the spectrum

of the sulfate anion SO_4^{--} but not the hydrogen sulfate anion HSO_4^-. This would indicate that oxidation of SO_2 on soot particles results in the formation of sulfate salt-like species with tetrahedral structure. The soot particle surface must in that case provide relatively strong basic sites for the neutralization of sulfuric acid.

References

1. T. Novakov, S. G. Chang, and A. B. Harker, Science 186, 259 (1974).
2. For details see S. G. Chang and T. Novakov, Lawrence Berkeley Laboratory Report LBL-4446 (1975).

Table I. Observed IRS fundamental vibrational frequencies of sulfate ions in the spectral region between 500 and 1500 cm^{-1}.

Origin	Main sulfur species	Pt. group	ν_1	ν_2	ν_3	ν_4
1N H_2SO_4	HSO_4^-	C_{3v}	885(S)	--	1040(S) 1160(S)	578(S) 605(M)
NH_4HSO_4 aqueous soln.	HSO_4^-	C_{3v}	860(S)	--	1035(S) 1162(S)	578(S) 605(M)
$(NH_4)_2SO_4$ aqueous soln.	SO_4^{--}	T_d	978(W)	--	1072(S)	612(M)
soot + SO_2 in humid air	SO_4^{--}	T_d	960(W)	--	1080(S)	615(M)

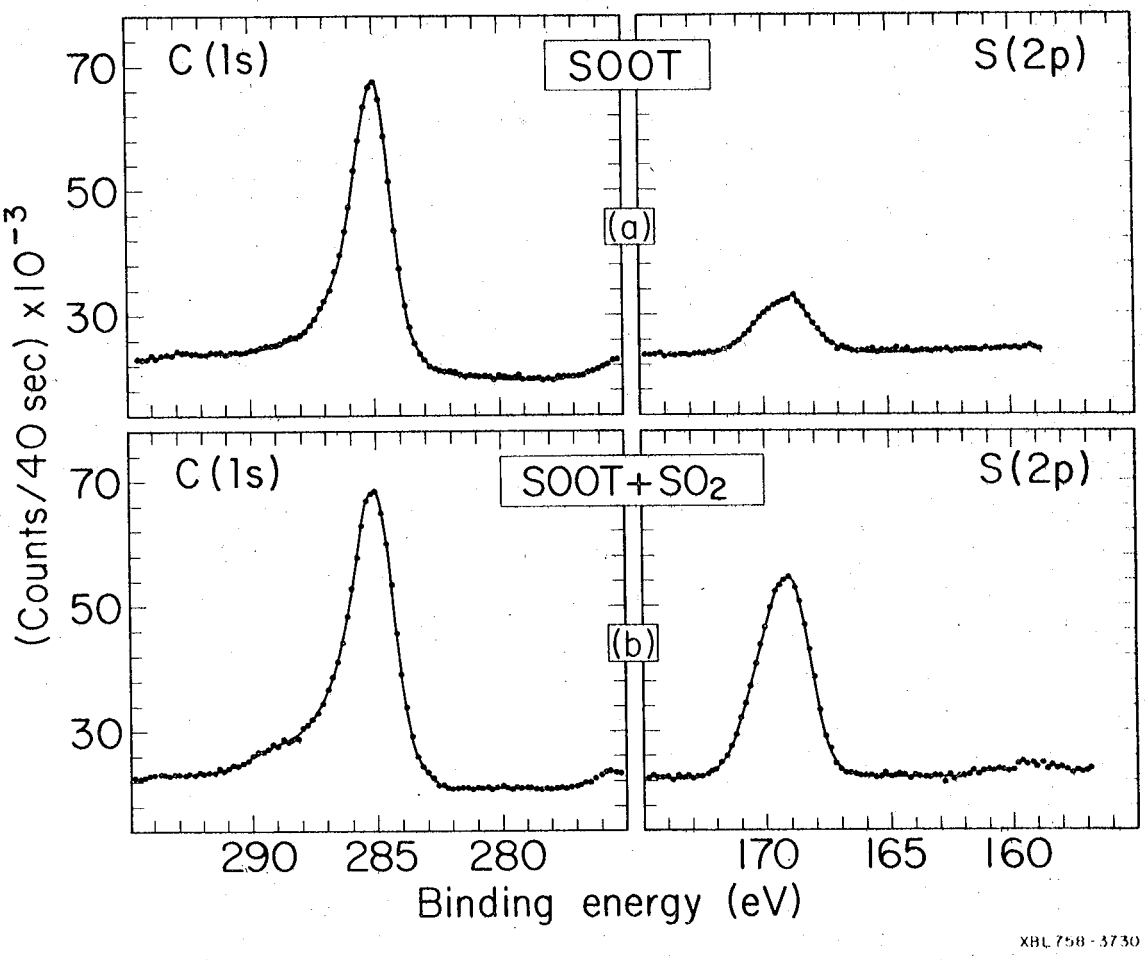

Figure 1. Carbon (1s) and sulfur (2p) photoelectron spectrum of (a) soot particles produced by combustion of propane saturated with benzene vapor. (The sulfur content of this fuel is 0.005% by weight.); (b) soot particles generated in analogous manner to (a), but exposed to additional SO_2 in humid air.

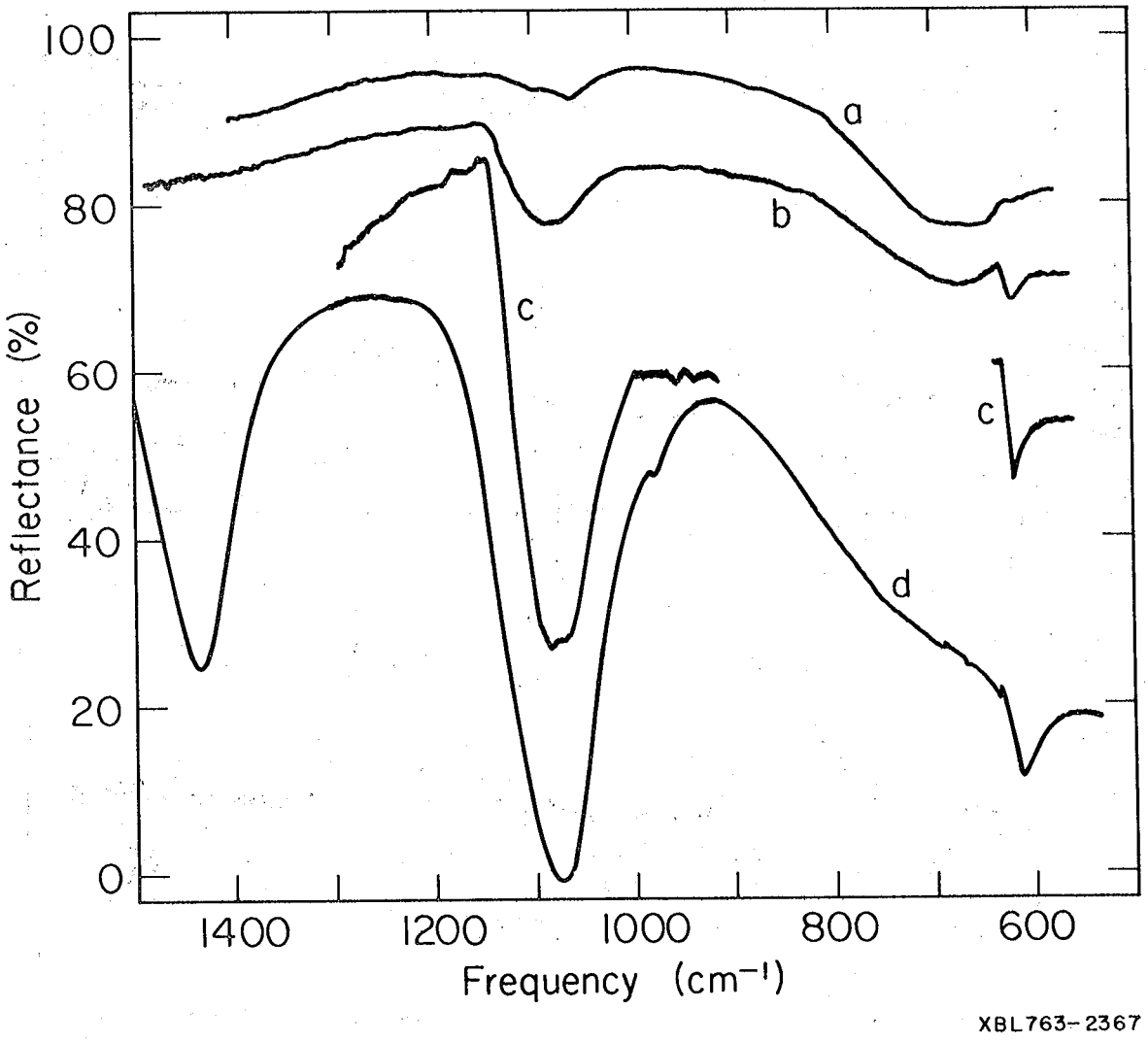

Figure 2. Infrared (IRS) spectra (between 1500 and 500 cm^{-1}) of (a) soot particles produced by combustion of propane saturated with benzene vapor; (b) soot particles generated in an analogous manner to (a), but exposed to additional SO_2 in humid air; (c) soot particles as in (b) but expanded by a factor of 5; (d) aqueous solution of ammonium sulfate (The absorption band at 1400 cm^{-1} is due to the ν_4 vibration of the NH_4^+ cation.).

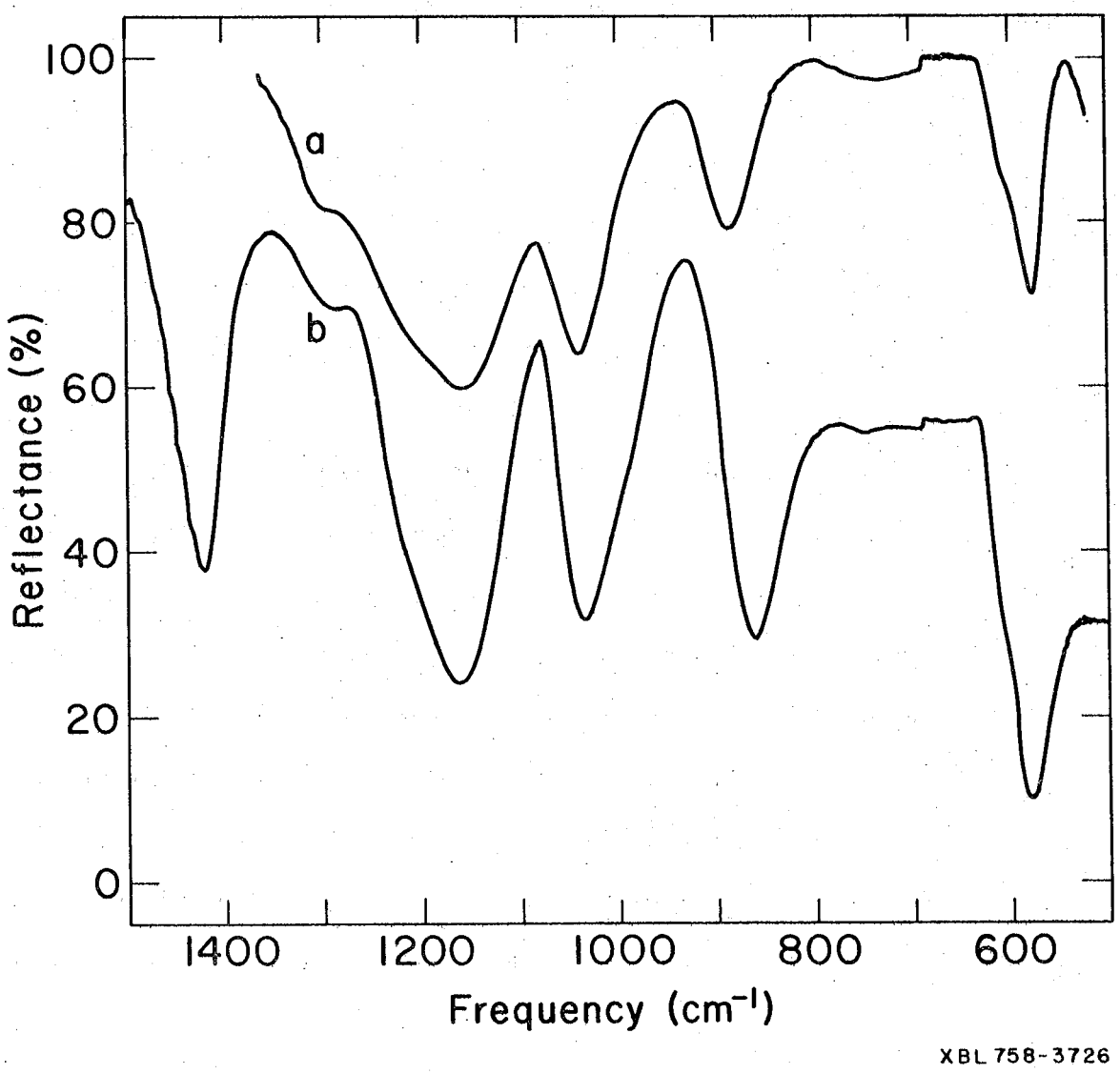

Figure 3. Infrared (IRS) spectra of (a) 1N sulfuric acid aqueous solution; (b) aqueous solution of ammonium bisulfate.

Possible Mechanism for the Catalytic Formation of Nitrates in the Atmosphere

S. G. Chang and T. Novakov

Nitric oxide is the major nitrogen pollutant produced by the combustion of fossil fuels. In the atmosphere NO can be oxidized to nitrates which are viewed as an environmental hazard. Most proposed mechanisms[1] require sunlight to initiate the reaction. There are many indications, however, that nitrates can be produced in heterogeneous nonphotochemical reactions. We have confirmed the presence of substantial nitrate concentrations by means of infrared spectroscopy and ESCA in the following cases: (a) soot particles from propane-benzene combustion in air; (b) exhaust particulates from an internal combustion engine; (c) airborne particles collected in a highway tunnel; and (d) activated carbon exposed to NO in humid air. As a result of these experimental findings and other available information, we have been able to propose a nonphotochemical step-by-step mechanism for the formation of nitrates. It should be emphasized, however, that more detailed experiments are necessary in order to establish the relative importance of this mechanism.

Infrared measurements were obtained using a Perkin-Elmer 621 spectrometer. The samples were mixed thoroughly with potassium bromide powder and pressed into pellets. The spectra between 1450 and 1300 cm^{-1} for the various samples are shown in Figures 1a, b, c, and d. In Figure 1e the spectrum of ammonium nitrate is shown for comparison. In all cases an intense and sharp band is found at 1385 ± 5 cm^{-1}. This band

corresponds to the ν_3 asymmetric stretching vibration of the NO_3^- anion. The broader band located at 1400 cm^{-1} is due to the ν_4 vibration of the NH_4^+ cation and its intensity relative to the nitrate absorption band varies considerably from sample to sample. Parallel measurements have been made using X-ray photoelectron spectroscopy (ESCA). These spectra verify the presence of nitrates in all the samples except the one taken in the Caldecott Tunnel where a large observed ammonium peak made the observation of the nitrate peak difficult.

Using some results of other workers we have been able to propose a step-by-step mechanism by which these nitrates may have been formed. As the starting point we use the work of Rao and Hougen[2] who showed that NO can be catalytically oxidized by activated carbon to NO_2, and the results of Smith[3] who proposed a rate law for the destruction of nitric acid by nitric oxide:

$$2HNO_3 + NO \xrightarrow{\text{surface}} 3NO_2 + H_2O$$

$$\frac{d(NO_2)}{dt} = k(HNO_3)(NO)(NO_2)$$

The equilibrium constant for the reaction is known, and by assuming the microreversibility of the reaction, we have derived the following rate equation for the formation of HNO_3:

$$\frac{d(HNO_3)}{dt} = k' \frac{(NO_2)^4(H_2O)}{(HNO_3)} ,$$

where k' is the rate constant and is a function of the nature of the

particle surface, k' = f(S). S represents the number of "active" sites on particle surfaces. Using this rate law as a guide, we propose the following step-by-step mechanism:

$H_2O + S \rightleftarrows H_2O \cdot S$	fast equilibrium
$2(NO_2 + NO_2 + M \rightleftarrows N_2O_4 + M)$	fast equilibrium
$N_2O_4 + H_2O \cdot S + S \rightleftarrows HNO_3 \cdot S + HNO_2 \cdot S$	fast equilibrium
$N_2O_4 + HNO_2 + S \rightleftarrows HNO_3 \cdot S + N_2O_3$	rate determining step
$N_2O_3 + M \rightleftarrows NO + NO_2 + M$	fast equilibrium
$H_2O + 3NO_2 + 2S \rightleftarrows 2HNO_3 \cdot S + NO$	overall reaction

Here M represents any third body; and $HNO_3 \cdot S$ represents the adsorbed HNO_3; $H_2O \cdot S$, adsorbed water, etc.

References

1. D. F. Miller and C. W. Spicer, J. Air Poll. Control Assoc. 25, 940 (1975).
2. M. N. Rao and O. A. Hougen, A.I.Ch.E. Symposium Series 48, 110 (1952).
3. J. H. Smith, J. Phys. Chem. 69, 1741 (1947).

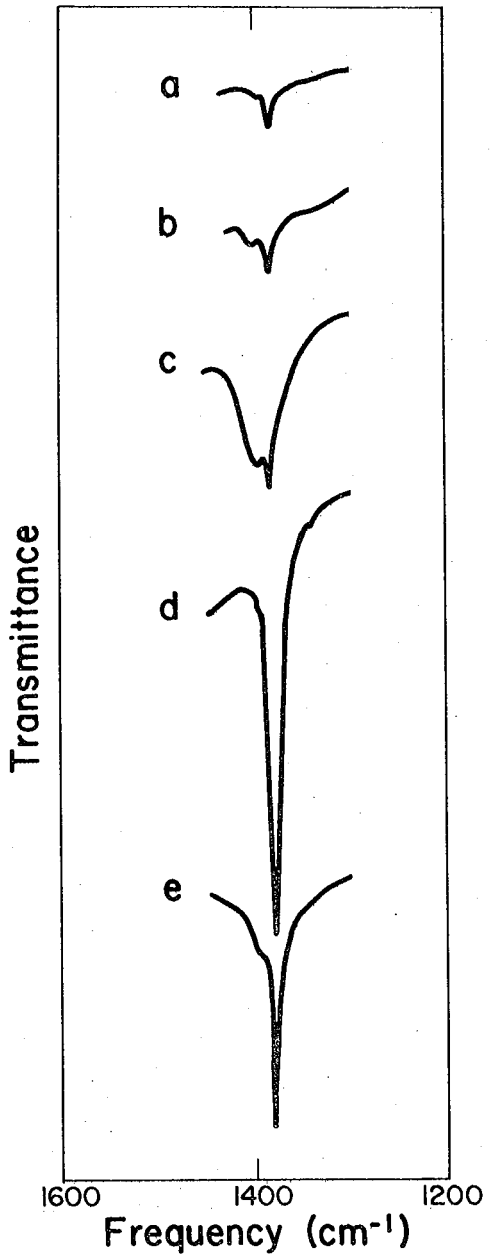

XBL 764-2612A

Figure 1. Infrared spectra between 1450 and 1300 cm^{-1} of a) soot particles from propane-benzene combustion in air; b) exhaust particles from an internal combustion engine; c) airborne particles collected in a highway tunnel; d) activated carbon exposed to NO in humid air; and e) ammonium nitrate.

SECTION III

FIELD STUDIES

Chemical and Physical Characterization of Vehicular Emissions

C. D. Hollowell, P. J. Bekowies, R. D. Giauque,
J. R. Wallace, and T. Novakov

The chemical and physical properties of gases and particles emitted by highway vehicles have been characterized in a highway tunnel which represents for the purpose of this study a "real-world," nonphotochemical reaction chamber for vehicular emissions. Studies were carried out in the Caldecott Tunnel, a vented, 3-bore, 6-lane, 1100-meter-long tunnel on a major San Francisco Bay Area commuter route with a traffic flow of about 10^5 vehicles per day.

This field program has three main purposes: (1) to characterize the chemical composition and understand the temporal variation of vehicular emissions; (2) to characterize the size distribution of the airborne particles; and (3) to elucidate the chemical and physical transformations of vehicular emissions under nonphotochemical conditions. Experiments were conducted at the tunnel roadway level of the uphill traffic bore ($\sim$ 4% grade), in the vent system, in nearby ambient air, and in a 600-m^3 tightly sealed room which could be flushed with ambient air, or filled with fresh, diluted vehicular emissions from the tunnel roadway.

1. Chemical Characterization and Temporal Variation of Vehicular Emissions

Particulate lead in ambient air has often been used as a tracer for gaseous and particulate air pollutants from automotive sources. An estimation of the contribution of vehicular sources (automobiles and trucks) to particulate carbon in ambient air is important for an assessment of their role in the particulate carbon chemistry of polluted air.

The specific purpose of these experiments was to study the carbon-to-lead ratio in order to assess the possibility of using lead as a tracer for particulate carbon from vehicles. It became immediately apparent that the C/Pb ratio was extremely variable as the ratio was found to vary over almost an order of magnitude.

Experiments were conducted to study the causes of deviation in the C/Pb ratio. An indication of the variability of the particulate emissions is seen by visual inspection of the fourth stage of a rotating drum Lundgren impactor[1] as shown in Figure 1. A large variation in particulate deposition as a function of time was observed. Several experiments were designed to measure C/Pb ratios during light mid-morning traffic ($\sim$ 50 mph), during rush-hour traffic (20-40 mph), during traffic stalls, as a function of the number of diesel trucks, and as a function of particle size. During these experiments the C/Pb ratio varied from 0.3 to 2.3 and was found to be highest during rush-hour and stalled-traffic periods. The C/Pb ratios correlated well with diesel truck traffic density according to Equation 1.

$$C/Pb = a + b(D/ND) \quad (1)$$

where D = number of diesel trucks per unit time

ND = number of nondiesel vehicles per unit time

a = .55 $\pm$.11 at 90% confidence level

b = 24 $\pm$5 at 90% confidence level

obtained by a least squares fit of numerous data points as shown in Figure 2.

These experiments clearly show that vehicular emissions of carbon and lead vary considerably with traffic conditions. Our results indicate

that Pb may be only marginally useful as a tracer for particulate carbon emitted by vehicles. The C/Pb ratio, for example, may follow a diurnal pattern in relation to the diurnal highway diesel truck density and general traffic conditions. The results also emphasize the importance of diesel trucks as a source of primary particulate carbon. On the average a 2% diesel traffic flow will yield a C/Pb ratio of 1.0. An increase in the diesel fraction to 10% will result in a C/Pb ratio of about 3. For zero diesel vehicles, the C/Pb ratio is about 0.5. The conclusion is therefore that an increase of the diesel fraction of the total vehicles from the current 2% to, for example, 10% would be equivalent to a sixfold increase in the number of nondiesel vehicles in terms of the primary carbon particulate loading.

From the observed carbon and lead concentrations, the above C/Pb relationship, and estimated airflows, emission rates were calculated. The "real-world" values calculated compared favorably with laboratory dynamometer test values as shown in Table I; however, since particulate emission rates vary markedly with driving conditions,[3,4] a direct comparison between results obtained under laboratory conditions and field conditions is difficult.

Gaseous vehicular emission rates for CO, NO_2, NO_x, and SO_2 were also calculated and are compared to Environmental Protection Agency emission rates in Table II. It should be noted that 10% of the total oxides of nitrogen in the tunnel roadway (nonphotochemical conditions) is NO_2.

2. Particle Size Distribution of Vehicular Emissions

Size fractionated particulate samples were collected at the roadway, in the tunnel exhaust venting system, and in nearby ambient air and were

analyzed for C, Pb, and Zn chemical composition. Samples were collected on the afterfilter (particle size < 0.5 μm) of a rotating drum Lundgren impactor in parallel with a total particulate sampler. Samples were also collected with an automatic dichotomous virtual impactor[5] which collects particles in two size fractions with a cut point at 2.4 μm. The results of these experiments showed that 75-90% of all particulate carbon and lead were present in particles smaller than 0.5 μm. The zinc concentrations at the roadway and in nearby ambient air exhibited a flat distribution with particle size. Zn/Pb ratios of 0.01 and 0.1 were observed at the tunnel roadway and in nearby ambient air, respectively. Thus vehicular traffic appears to be an unimportant source of ambient zinc.

Essentially all carbon and lead generated by vehicular highway traffic is in the submicron size range and should be considered a direct combustion product. "Tire dust" does not appear to be an important source of carbon from vehicular traffic; this is in contrast to the estimates of Friedlander[6] who considers tire dust to be a major source of primary particulate carbon from vehicles.

3. Chemical and Physical Transformations of Vehicular Emissions

Tunnel roadway air containing fresh vehicular emissions was sealed in a 600-m^3 room for 2.5 hours and analyzed for particulate C, Pb, and S as well as CO and SO_2. The experiment was repeated at relative humidities in the range of 65-100% and temperatures from 17° to 22°C. No change in concentration of the above species was observed in the 2.5-hour period. Further studies will follow the concentrations of these species over

periods of 12 to 24 hours to study the oxidation of SO_2 to sulfur-containing aerosol. Recent work[7,8,9] has reported this conversion rate in power plant plumes to be from 1.5%/hr to 5%/hr, a rate which could be observed in our experiment only after many hours due to relatively low SO_2 levels in the tunnel.

An electrical aerosol size analyzer (EASA)[10] was used to measure the size distribution of fresh and aged aerosols at the tunnel roadway and in the sealed room filled with vehicular emissions. Surface distributions calculated from the EASA data showed two prominent modes: one at about 0.02 μm and another at 0.1 to 0.2 μm. This bimodal distribution was observed to vary with time in the sealed room, filled initially with fresh vehicular emissions. The 0.02-μm mode was found to decrease rapidly with time, while the 0.1-to-0.2-μm mode decreased at a much slower rate. A simple model was used to show that coagulation of the aerosols was the dominate mechanism governing changes in the size distribution. This model successfully explained the observed time evolutions and the relative intensities of the two modes.

References

1. D. A. Lundgren, J. Air Pollut. Contr. Assoc. 17, 225 (1967).
2. Compilation of Air Pollution Emission Factors, U.S. Environmental Protection Agency, Publication AP-42 (September, 1973 and December, 1975).
3. G. I. Ter Haar, D. L. Lenane, J. N. Hu, and M. Brandt, J. Air Pollut. Contr. Assoc. 22, 39 (1972).
4. K. Habibi, Environ. Sci. Technol. 7, 223 (1973).

5. F. S. Goulding, J. M. Jaklevic, B. M. Loo, Fabrication of Monitoring System for Determining Mass and Composition of Aerosol as a Function of Time, Report UCID-3767, Lawrence Berkeley Laboratory, University of California, Berkeley, CA 94720; Report EPA-650/2-75-048, U.S. Environmental Protection Agency, Washington, DC 20460 (April, 1975).

6. S. K. Friedlander, Environ. Sci. Technol. 7, 235 (1973).

7. L. Newman, J. Forrest, and B. Manowitz, Atmos. Environ. 9, 969 (1975).

8. R. B. Smith and G. H. Jeffrey, Atmos. Environ. 9, 643 (1975).

9. K. T. Whitby, B. K. Cantrell, R. B. Husar, N. V. Gillani, J. A. Anderson, D. L. Blumenthal, and W. E. Wilson, Jr., Aerosol Formation in a Coal Fired Power Plant Plume (unpublished report, 1976).

10. B. Y. H. Liu, K. T. Whitby, and D. Y. H. Pui, A Portable Electrical Aerosol Analyzer for Size Distribution Measurement of Sub-Micron Aerosols, presented at the 66th Annual Meeting of the Air Pollution Control Association, Chicago, Illinois, June 24-28 (1975).

Table I. Carbon and lead vehicular emission rates.

Vehicles	C (g/mile)	Pb (g/mile)
This work		
Nondiesel vehicles	0.07 ±.03	0.13 ±.05
Diesel trucks	1.7 ±.8	0.0
Previous work		
Automobiles	0.076[a]	0.08-0.20[b,c]
Diesels	1.3[d]	0.0

[a]Ref. 3, hot cycle conditions.

[b]Ref. 3.

[c]Ref. 4.

[d]Ref. 2, assuming diesel particulate emissions to be 100% carbon.

Table II. CO, NO_2, NO_x, and SO_2 vehicular emission rates.

Vehicles	CO (g/mile)	NO_2 (g/mile)	NO_x (g/mile)	SO_2 (g/mile)
This work				
All vehicles	40 ±15	0.5 ±.2	6 ±2	0.3 ±.1
EPA emission factors[2]				
1975 highway vehicle population at 45 mph	25	—	6.5	0.20

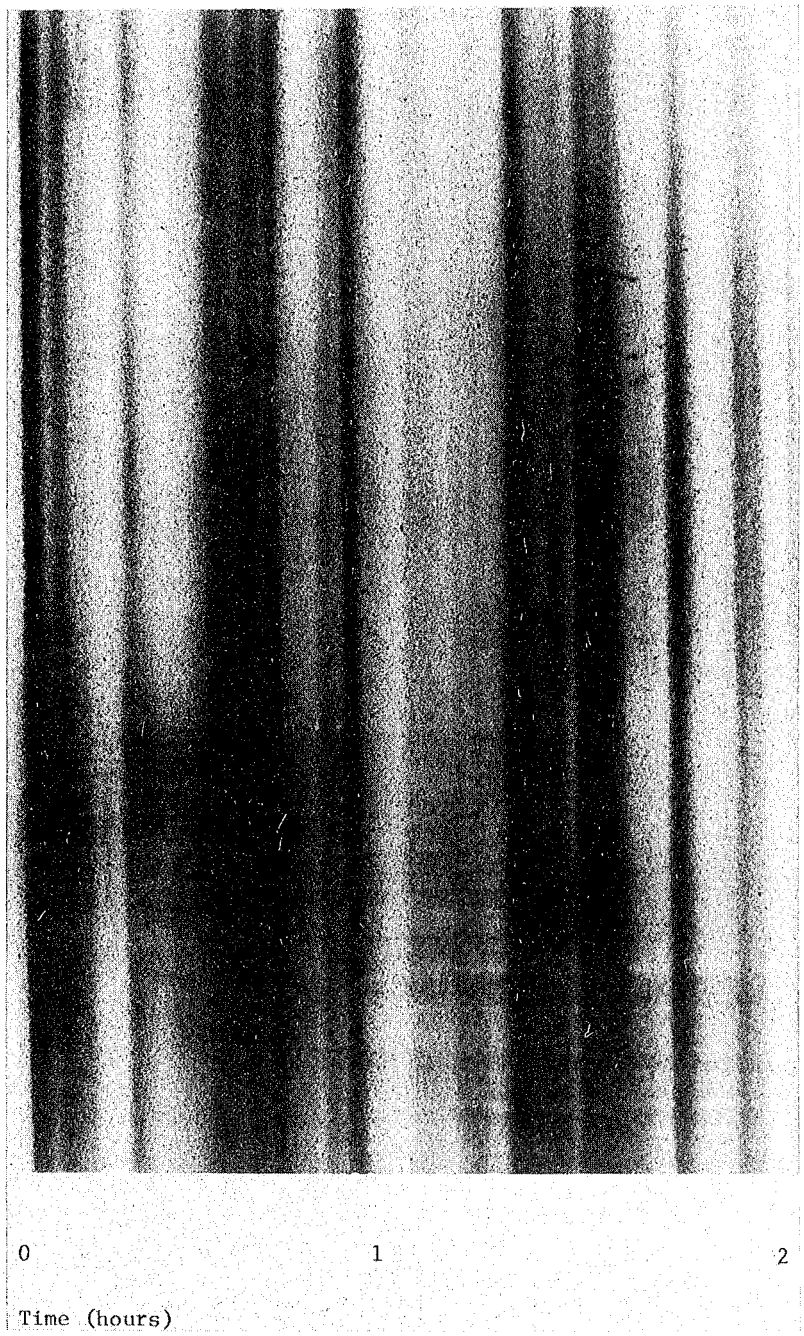

XBB 7510-7496A

Figure 1. Photograph of the particulate deposition collected as a function of time on the fourth stage (particle size range 0.5-1.5 μm for particles of unit density) of a rotating drum Lundgren impactor. Banded structure is caused by temporal variations in the vehicular emissions.

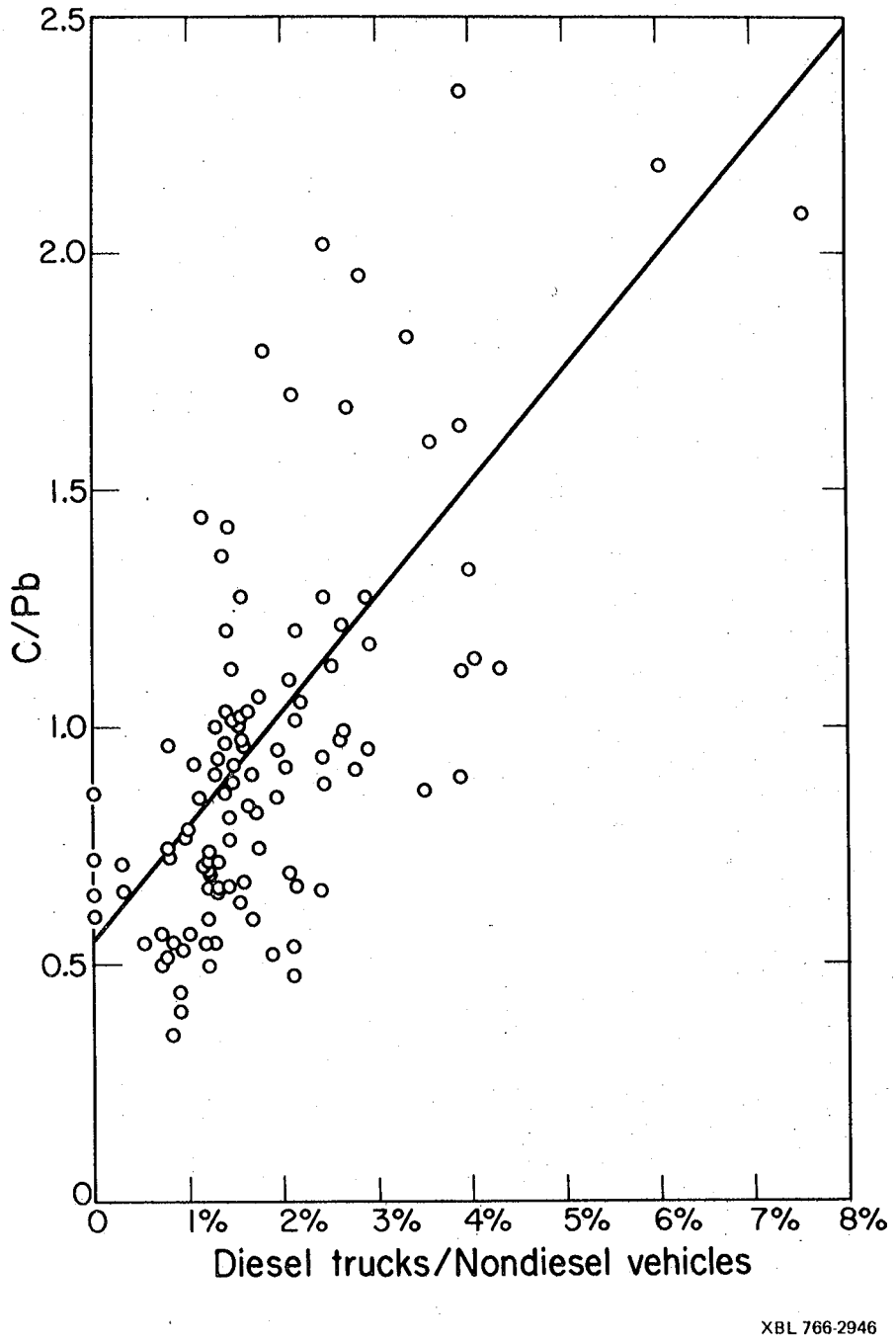

Figure 2. Measured C/Pb ratios as a function of percent of diesel trucks. The straight line is obtained by a least squares fit to the data and is represented by

$$C/Pb = .55(\pm.11) + 24(\pm5)\cdot\left(\frac{\#\text{ diesel trucks}}{\#\text{ nondiesel vehicles}}\right).$$

Mobile Atmospheric Research Laboratory

C. D. Hollowell and T. Novakov

The Mobile Atmospheric Research Laboratory (MARL) has been designed to provide a comprehensive atmospheric characterization and monitoring laboratory for field air pollution studies. The laboratory is a self-contained unit capable of supporting field studies at almost any location and is readily movable to new sampling sites without requiring extensive time and effort. The design has sufficient flexibility to allow changes to new or different equipment. MARL is a compact facility (approximately the size of a mobile home van) which is large enough to contain a complete array of gaseous and aerosol measuring instruments, yet small enough to be very maneuverable and easily accommodated in small spaces. It is designed so that field measurements can be made reliably and efficiently with minimum effort. Figures 1 and 2 show exterior and interior views of MARL.

MARL contains the latest state-of-the-art air pollution monitoring equipment, meteorology instrumentation, calibration equipment, and data acquisition system necessary for routine and fundamental research characterization and monitoring studies. The parameters measured and instrumentation are given in Table I. The equipment is fixed in MARL for ground field studies or is easily removed for aerial or laboratory studies.

An automatic computer data acquisition and control system is currently being installed. All of the continuous monitoring instrument outputs will be digitized and stored on magnetic tape. In addition, the

computer system will synchronize the timing and control of the instruments so that samples are taken only after the individual systems are calibrated and stabilized. The computer system will initially accommodate 48 monitors and 48 controls with the ability to run in an unattended mode for up to 48 hours. Real time reduction of data falls entirely within the capabilities of this system; however, the initial goal is to transport all raw data to the LBL Computer Center for analysis.

Other salient features of MARL are listed below.

- The laboratory unit is an insulated, air conditioned, and heated aluminum body fitted onto a Ford F350 1-1/2-ton truck.
- The overall truck dimensions are 2.4 m W × 6.6 m L × 3.6 m H, and the laboratory dimensions are 2.4 m W × 3.6 m L × 2.1 m H.
- The roof is a working platform containing meteorology and aerosol sampling equipment.
- Double rear doors allow easy loading and unloading of major equipment.
- The instrument rack mounting space is 7.2 m; 5.4 m of rack space is suspension mounted and accessible from all sides.
- A special compartment below the floor of the truck body is used to house vacuum pumps and insulate their noise from the laboratory.
- The electric power requirement configuration is a 200-V, 25-A, 3-phase, 4-conductor cable system for hook-up to external installed power supply or self-contained generator.
- A 5-kW diesel generator on a towed trailer with 100-m extension for downwind location is available for self-contained operation.

Several programs currently in progress or proposed will utilize the Mobile Atmospheric Research Laboratory. Some of these programs are outlined below.

- The Atmospheric Aerosol Field Studies are designed to assess the role of heterogeneous gas-particle reactions in the formation and evolution of aerosol air pollution in ambient air, stationary source, and mobile source environments.
- The Indoor Air Pollution Study is designed to assess the extent of indoor-generated air pollution and conduct epidemiology studies on the disease effects of indoor pollutants.
- The Geothermal Field Study is designed to assess the emission of gaseous and aerosol air pollutants, their transport, and transformation from geothermal energy sites.

Table 1. Mobile Atmospheric Research Laboratory--parameters measured and instrumentation.

Parameter Measured	Principle of Measurement	Manufacturer/Model	Status 2/1/76
Sampling Equipment			
Gases and Aerosols	Aluminum and stainless steel sampling intake and manifold to continuous monitoring instruments and filter sampling equipment	LBL	In progress
Gases	Multi-point automatic electronic sequential sampler with Teflon sampling lines	LBL	Proposed
Aerosols			
Size-fractioning aerosol filter sampling equipment for laboratory mass distribution and chemical composition analysis by β-gauge and XRF	Automatic dichotomous virtual impactor (2.4 μm cut point)	LBL	Installed
	Manual dichotomous virtual impactor (3.5 μm cut point)	Sierra Instruments 243	Proposed
	4-stage Lundgren impactor with 0.3, 1, 3 and 10 μm cut-offs	Sierra Instruments 4220	Proposed
Total aerosol filter sampling equipment for laboratory chemical composition analysis by XRF, ESCA, IR, combustion techniques (for C/H/N analysis) and wet chemistry	Pump with 47 mm filter holder	3 LBL Systems	Installed
	High volume sampler	Sierra Instruments Ultra Vol	Installed
Continuous Monitoring Instruments			
Gases			
SO_2	UV Fluorescence	Thermo Electron 43	Installed
$NO/NO_2/NO_x$	Chemiluminescence	Thermo Electron 14D	Installed
O_3	UV Absorption	Dasibi 1003-AAS	Installed
CO	NDIR	Beckman 7000	Installed
Hydrocarbons	GC/FID		Proposed
NH_3	Chemiluminescence	Thermo Electron, LBL	Proposed
H_2S	GC/FPD	Tracor 270H	Proposed
Aerosols			
Size (0.01 1μm)	Condensation Nuclei Formation	Environment/One Rich 100	Installed
(0.01 1μm)	Electrical Mobility Analysis	Thermo Systems 3030	Installed
(0.3 20μm)	Optical Counting	Royco 225	Proposed
b_{scat}	Nepholometry	MRI 1550 LBL	Installed In progress
Zero, Span and Calibration Equipment			
Gases			
Zero/CO/NO/NO_2/SO_2	Scrubbers, Gas Cylinders, Dilution System, and Permeation Tubes	Monitor Labs 8500	Installed
O_3/NO/NO_2	Gas Phase Titration		Proposed
Meteorology Instruments			
Wind Speed	Generator	Young 3 Cup Anemometer 6101	Installed
Wind Direction	Potentiometer	Young Wind Vane 6301	Installed
Temperature	Thermistor	Singer 84R with 2 remote sensors	Installed
Dew Point	Thermoelectric Cooling/Resistance Measurement	Singer 84R with 2 remote sensors	Installed
Total Solar Radiation	Spectral Pyranometer Thermopile	Eppley PSP	Proposed
UV Radiation	UV Radiometer Photoelectric Cell	Eppley TUVR	Proposed
Pressure	Potentiometer		Proposed
Data Acquisition Equipment			
Analog Output	Strip Chart Recording	Soltec 6 Pen Recorder	Installed
		3 Heathkit Recorders	Installed
Automated Data Acquisition System	A/D Converter; Magnetic Tape Recorder		Proposed

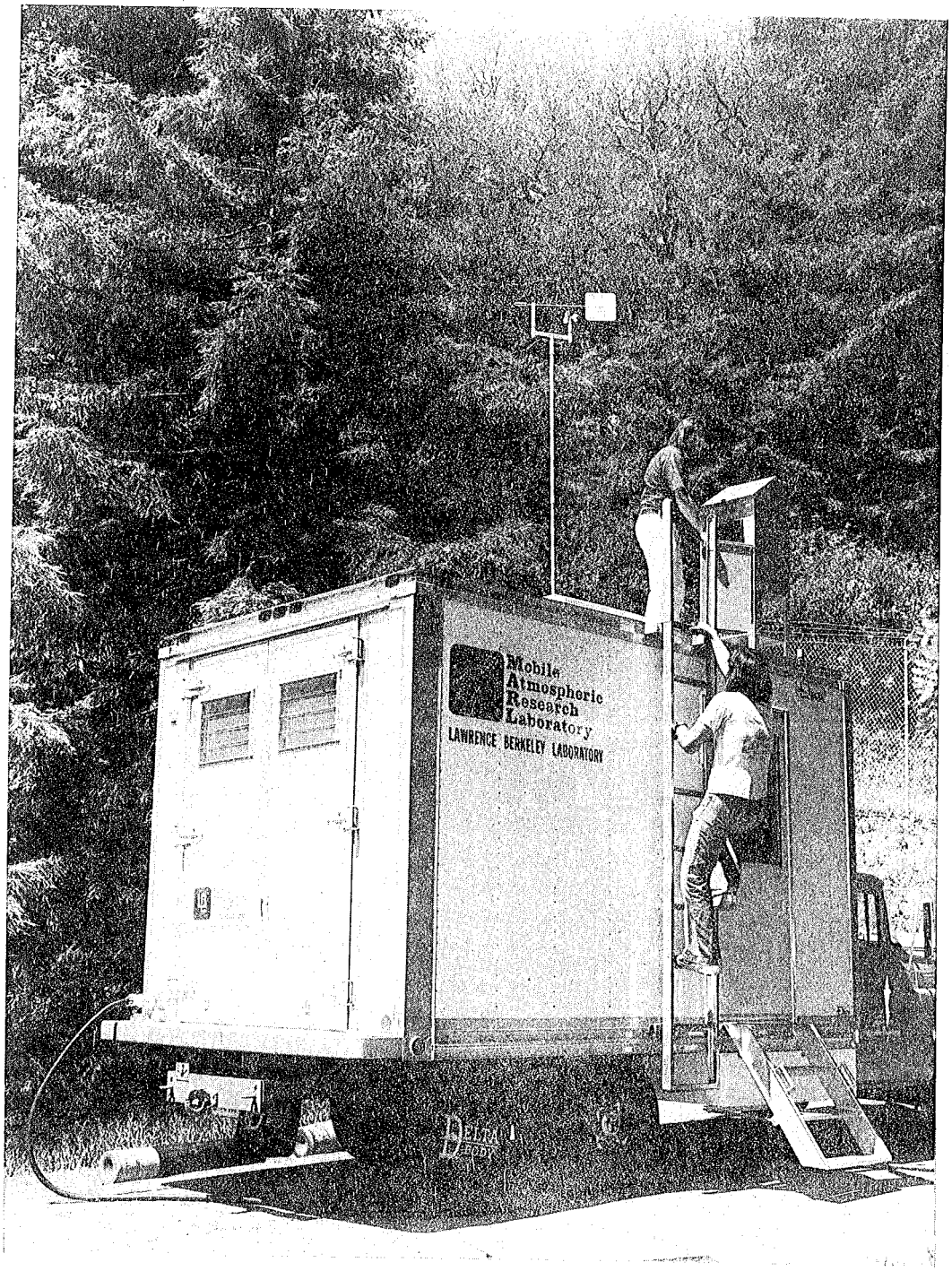

CBB 766-5702

Figure 1. Exterior view of Mobile Atmospheric Research Laboratory.

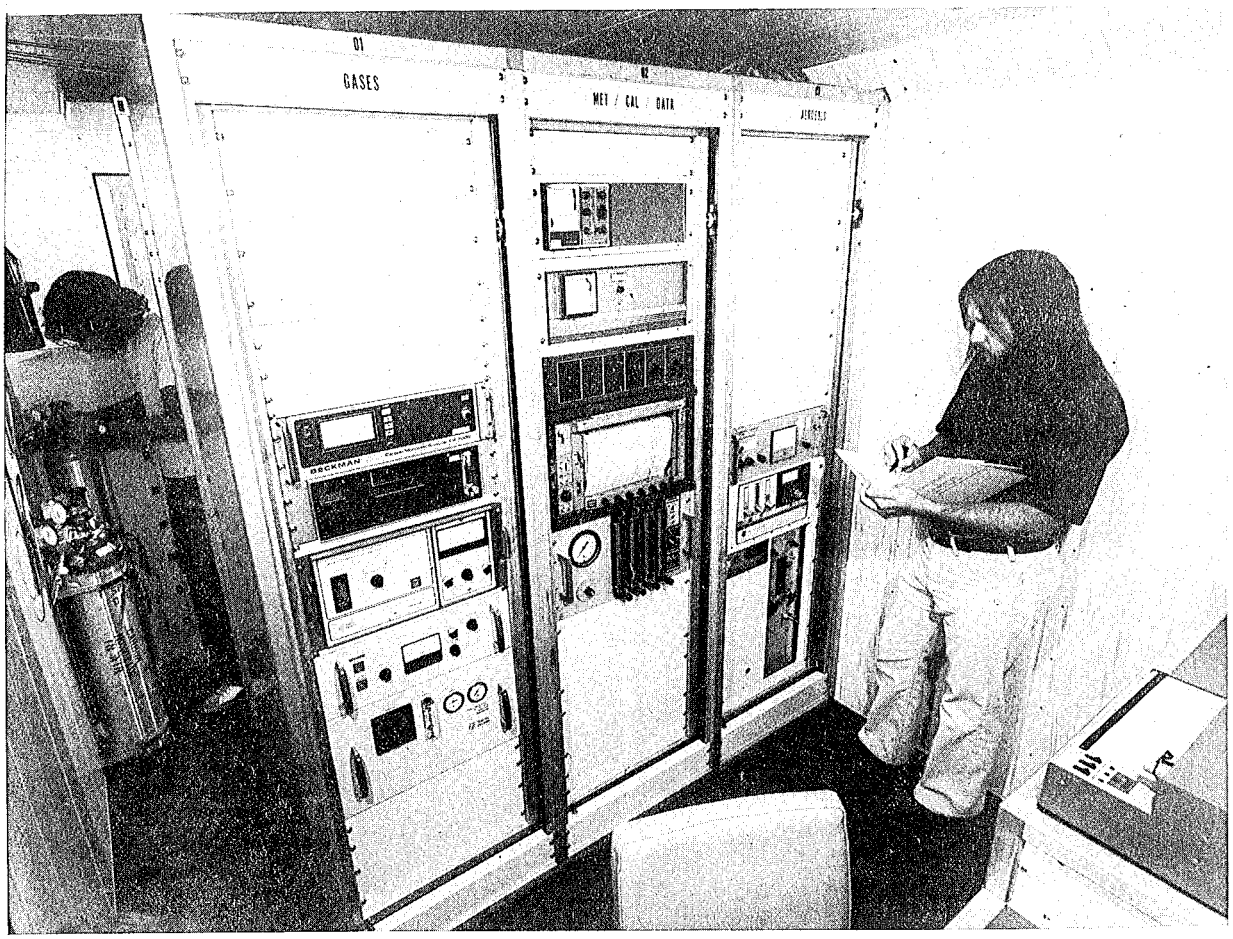

CBB 766-5704

Figure 2. Interior view of Mobile Atmospheric Research Laboratory showing the main instrument racks.

This report was done with support from the United States Energy Research and Development Administration. Any conclusions or opinions expressed in this report represent solely those of the author(s) and not necessarily those of The Regents of the University of California, the Lawrence Berkeley Laboratory or the United States Energy Research and Development Administration.